Engineering 23 (2023) 40–55

Contents lists available at ScienceDirect

Engineering

journal homepage: www.elsevier.com/locate/eng

Research
Materials for Molecular Separations—Review

Mixed-Matrix Membranes Containing Porous Materials for Gas Separation: From Metal–Organic Frameworks to Discrete Molecular Cages

Ziqi Yang [a], Zhongjie Wu [a,b], Shing Bo Peh [a], Yunpan Ying [a], Hao Yang [a], Dan Zhao [a,*]

[a] Department of Chemical and Biomolecular Engineering, National University of Singapore, Singapore 117585, Singapore
[b] Joint School of the National University of Singapore and Tianjin University, International Campus of Tianjin University, Fuzhou 350207, China

ARTICLE INFO

Article history:
Received 30 December 2021
Revised 19 May 2022
Accepted 3 July 2022
Available online 8 March 2023

Keywords:
Gas separation
Metal–organic frameworks
Metal–organic cages
Mixed-matrix membranes
Interfacial compatibility

ABSTRACT

Mixed-matrix membranes (MMMs), which combine porous materials with a polymeric matrix, have gained considerable research interest in the field of gas separation due to their complementary characteristics and cooperative activation. The tailorability and diversity of porous materials grant MMMs extendable functionalities and outstanding separation performance. To achieve the full potential of MMMs, researchers have focused on the rational matching of porous fillers with polymeric matrixes to achieve enhanced compatibility at the interfaces of these materials. In this review, we highlight state-of-the-art advances in combining metal–organic frameworks (MOFs) and metal–organic cages (MOCs) with polymeric matrixes to fabricate MMMs using different strategies. We further discuss the opportunities and challenges presented by the future development of MMMs, with the aim of boosting MMM fabrication with judicious material design and selection.

1. Introduction

Gas separation is an essential industrial process. Compared with conventional separation processes such as distillation and absorption, membrane-based gas separation is a powerful approach that can be used in various applications to alleviate global environmental and energy crises [1–4]. The first commercialized membrane-based gas separation system was installed in 1980 for hydrogen (H_2) separation [5]. At present, membrane-based gas separation is diversified to include carbon dioxide (CO_2) capture, natural gas sweetening, H_2 production and purification, olefin/paraffin separation, and other petrochemical-related applications [6–10]. Diverse membrane materials have been developed to achieve outstanding separation performance, including inorganic membranes, two-dimensional (2D) lamellar membranes, and polymeric membranes [11–20]. Polymeric membranes dominate the current gas separation market due to their low cost, easy processability, and high reproducibility [11,20]. However, the separation performance of polymeric membranes is usually constrained by the tradeoff relationship between permeability and selectivity; that is, more permeable polymers are usually less selective and vice versa (Fig. 1) [21–24]. This tradeoff is known as the "Robeson upper bound."

The incorporation of porous fillers into a polymeric matrix has inspired the development of polymer/filler hybrid membranes—the so-called mixed-matrix membranes (MMMs) [25]. MMMs integrate the advantages of the flexibility and processability of polymers with the precision of porous fillers, resulting in high permeability and selectivity [25–28]. Although some MMMs exhibit superior separation abilities, their current performance is still far from the predicted values, since the rational matching of porous fillers and polymeric matrix is challenging. As a result, unfavorable morphologies can be generated in MMMs, including filler particle aggregation, nonselective interfacial voids, polymer chain rigidification, and filler pore blockage (Fig. 2) [13,26,27]. Aggregation of filler particles will produce nonselective voids or even macroscopic defects within the membrane, leading to decreased separation selectivity. Interfacial voids will form a bypass for gas molecules, resulting in negligible or even no separation selectivity. Polymer chain rigidification around fillers will create a barrier to gas transport due to lower polymer chain mobility, leading to decreased permeability, which is commonly encountered in rubbery

* Corresponding author.
E-mail address: chezhao@nus.edu.sg (D. Zhao).

https://doi.org/10.1016/j.eng.2022.07.022

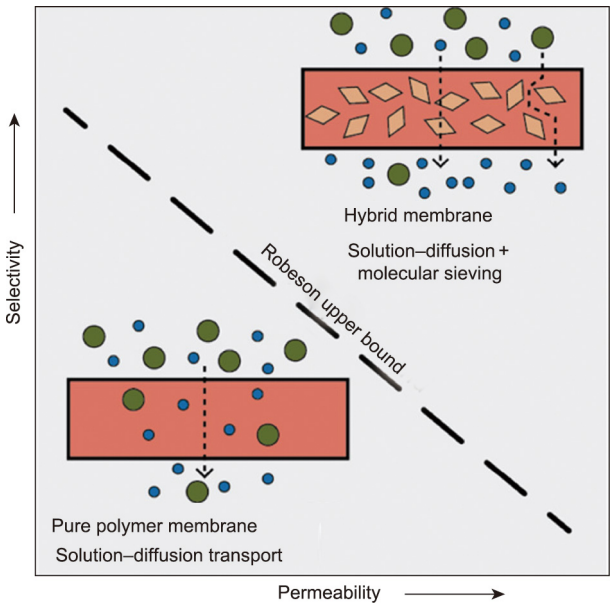

Fig. 1. Schematic representation of the tradeoff relationship between permeability and selectivity. Reproduced from Ref. [24] with permission.

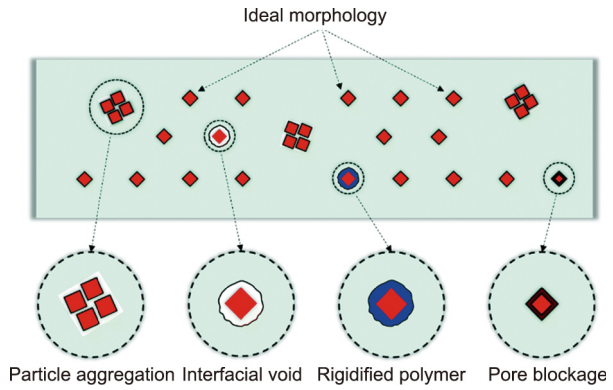

Fig. 2. Schematic diagram of fabricated MMMs and the formation of unfavorable morphologies in MMMs. Reproduced from Ref. [27] with permission.

polymer-based MMMs [29,30]. The pore-blocking of fillers by polymer chains or solvent molecules can turn porous fillers into impermeable particles, resulting in increased path tortuosity for gas transport and thus decreased permeability [13,31–33].

To mitigate these problems and fulfill the potential of MMMs, researchers have proposed numerous strategies for the rational matching of porous materials with polymeric matrixes to achieve improved interfacial morphology and compatibility [13,27,29]. Such approaches include adjusting the geometry and functionality of porous fillers and building connections between porous fillers and the polymeric matrix by forming electrostatic interactions, hydrogen bonds, coordination bonds, or even covalent bonds. The selected porous fillers include metal–organic frameworks (MOFs), covalent organic frameworks (COFs), porous aromatic frameworks, metal–organic cages (MOCs), and so forth [26,34–36]. MOFs, which possess tunable pore architectures, high stability, and diverse designability, are among the most studied porous fillers in MMMs and show excellent separation performance [26]. MOCs, which are discrete molecular compounds, are emerging porous fillers in this field [36]. Although they have not been studied extensively, their good solubility and processability endow MOCs with the potential capability to achieve homogeneous dispersion and good compatibility with polymeric matrixes at the molecular level, which could solve the long-standing interfacial issues of MMMs [36,37]. Considering the similarities between MOFs and MOCs, we provide a comprehensive overview of recent advances in MMMs containing MOFs and MOCs as porous fillers for gas separation. We discuss the strategies that have been developed for the fabrication of MOF-/MOC-based MMMs with enhanced interfacial compatibility and separation performance. Furthermore, we highlight the challenges and perspectives that may deserve consideration for the future development of MMMs. We hope that this review will inspire the design and selection of membrane materials and the construction of high-performance MMMs.

2. Types of porous materials

2.1. Metal–organic frameworks

MOFs are hybrid porous materials composed of metal ions or clusters that are coordinated with organic linkers via coordination bonds to form extended crystalline structures [38–40]. Typical MOFs used in MMMs include zeolitic imidazolate frameworks (ZIFs), University of Oslo-66 (UiO-66) series, and Materials Institute Lavoisier (MIL) series (Fig. 3) [26,33]. ZIFs are composed of transition metal cations (e.g., Zn^{2+}, Co^{2+}) and anionic imidazolate linkers, with a structure resembling that of zeolites [41,42]. By changing the anionic imidazolate linkers, a series of ZIFs with different aperture sizes, such as ZIF-8 (0.34 nm) and ZIF-90 (0.35 nm), have been prepared and incorporated into polymeric matrixes for MMM fabrication [41,43–46]. Among them, ZIF-8, which is composed of Zn^{2+} and 2-methylimidazole linker, has been investigated in depth for membrane-based gas separation, especially for propylene/propane (C_3H_6/C_3H_8) separation [41,47,48]. UiO-66 is another popular porous filler that exhibits excellent stability in aqueous solutions and various organic solvents [38]. The original UiO-66, which is composed of terephthalic acid (BDC) linker, possesses octahedral and tetrahedral cavities [26,38]. By replacing the linker with other BDC derivatives, a series of UiO-66-type MOFs with different functional groups (e.g., $–NH_2$, –OH, $–SO_3H$) were obtained [49–54]. UiO-66-NH_2, a type of amine-functionalized MOF, is particularly attractive owing to its inherent basic properties that afford good affinity toward acid gases and allow further modifications [29,38]. MIL-series MOFs exhibit interesting properties such as flexibility, high surface area, and high stability, introducing new possibilities when used as fillers in MMM fabrication

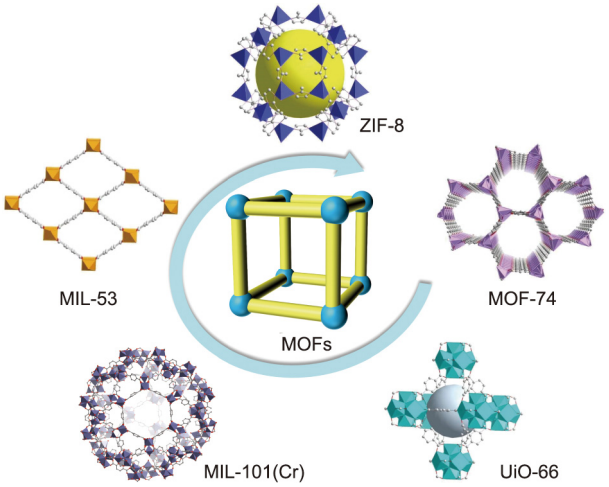

Fig. 3. Crystal structures of the representative MOFs used in MMMs.

[55–58]. For example, MIL-53 is known to have a "breathing" effect, which manifests as a structural transformation from narrow pores to large pores when adsorbing guest molecules [26,55]. MIL-101(Cr), which has large mesoporous cavities (2.9 and 3.4 nm), possesses a high surface area, excellent hydrothermal stability, and a high CO_2 uptake of 40 mol·kg^{-1} (at 304 K and 5 MPa) [53,57,59].

2.2. Metal–organic cages

MOCs, also referred to as metal–organic polyhedra (MOPs), are a class of discrete molecular assemblies formed by coordination bonds between metal nodes and organic ligands [60–64]. Unlike MOFs, MOCs do not form extended frameworks. When MOCs are dissolved, discrete MOC molecules can be present in solutions, since no bonds need to be broken [65]. Zirconium-based MOCs (Zr-MOCs), which are composed of trinuclear zirconium clusters and carboxylate ligands, have gained increasing scholarly attention due to their outstanding aqueous and chemical stability [64,66,67]. Bis(cyclopentadienyl)zirconium dichloride (Cp_2ZrCl_2) is the most commonly used zirconium (Zr)-based reagent in the synthesis of Zr-MOCs, wherein the cyclopentadiene (Cp) group at the vertices prevents the extended assembly of cages (Fig. 4(a)) [68]. By tuning the ligand type, researchers have successfully synthesized Zr-MOCs with different functional groups (e.g., $-NH_2$, $-SO_2$, $-SO_3Na$), which are expected to aid in the building of crosslinked networks and enhance the networks' affinity to the gases of interest during separation [63,68–71]. In particular, amino-functionalized Zr-MOC (i.e., ZrT-1-NH_2), which is synthesized from Cp_2ZrCl_2 and 2-aminoterephthalic acid (NH_2-BDC), has been studied widely for the fabrication of membranes and extended architectures (Fig. 4(a)) [66,68,71,72]. The ionic character of Zr-MOC renders it soluble in organic solvent/water mixed systems, such as *N*,*N*-dimethylformamide (DMF)/water, methanol/water, acetone/water, and acetonitrile/water [66].

Copper-based MOCs (Cu-MOCs), which are composed of 12 dinuclear Cu(II) paddlewheel units and 24 bridging linkers, have a cub-octahedral structure (Fig. 4(b)) [63,73]. The first Cu-MOC was synthesized in 2001 using isophthalic acid (IPA) as the ligand [74]. Subsequently, a series of Cu-MOCs were successfully synthesized by functionalizing the 5-position of the IPA ligand [61,62,75]. The introduction of long alkyl chains or polyethylene glycol (PEG) chains on the ligand has proven to be an efficient way to increase the solubility of Cu-MOCs in commonly used organic solvents, such as tetrahydrofuran (THF), dichloromethane (DCM), and DMF [65,76–79]. Cu-MOCs usually have poor hydrolytic stability and thus suffer from decomposition in the presence of water, which restricts their application in water-related systems [73,77,80]. In contrast to Cu-MOCs, isostructural rhodium-based MOCs (Rh-MOCs) possess high hydrolytic stability due to the robust Rh–Rh bonds in the paddlewheel units (Rh–Rh bond energy: 16.5 kcal·mol^{-1}, 1 kcal ≈ 4184 J) [81]. The activity of the axial Rh–Rh paddlewheels and the structural stability of Rh-MOCs allow researchers to modulate the solubility and functionality of Rh-MOCs by means of either post-assembly modification (PAM) or coordination with N-donor molecules, which provides opportunities for the construction of MOC-based functional materials with well-defined porosity [82,83].

The design and selection of MOCs with excellent stability are necessary for MMM industrial applications. CO_2 capture—one of the most important separation applications for MMMs—involves issues of water stability. MOCs with poor hydrolytic stability will undergo structural collapse and therefore lose their separation abilities when challenged with real flue gas. To address this issue, PAM is a useful strategy for overcoming the poor stability of MOCs constructed by labile metal ions, such as Cu^{2+} [63,84]. Decorating a hydrophobic shielding layer onto the outer surface of MOCs or crosslinking neighboring MOCs to construct stronger coordination bonding may help stabilize the porous structure, although this may sacrifice the solution processability of MOCs to some extent [85,86].

3. Fabrication of MMMs

As the library of MOFs and MOCs grows, more advanced MMMs using MOFs or MOCs as porous fillers have been developed [26,34,36,87,88]. Appropriate combination methods for porous fillers and polymers are essential in realizing favorable interfacial compatibility and excellent separation performance [25,27]. Herein, we classify the strategies for fabricating MOF-/MOC-based MMMs into two categories: fabrication strategies using physical mixing; and fabrication strategies using covalent linkages. The former involves a simple mixture with only spontaneous or weak interactions (e.g., electrostatic interactions, coordination bonds, and hydrogen bonds) at the interface, while the latter involves covalent bonds between porous fillers and polymers.

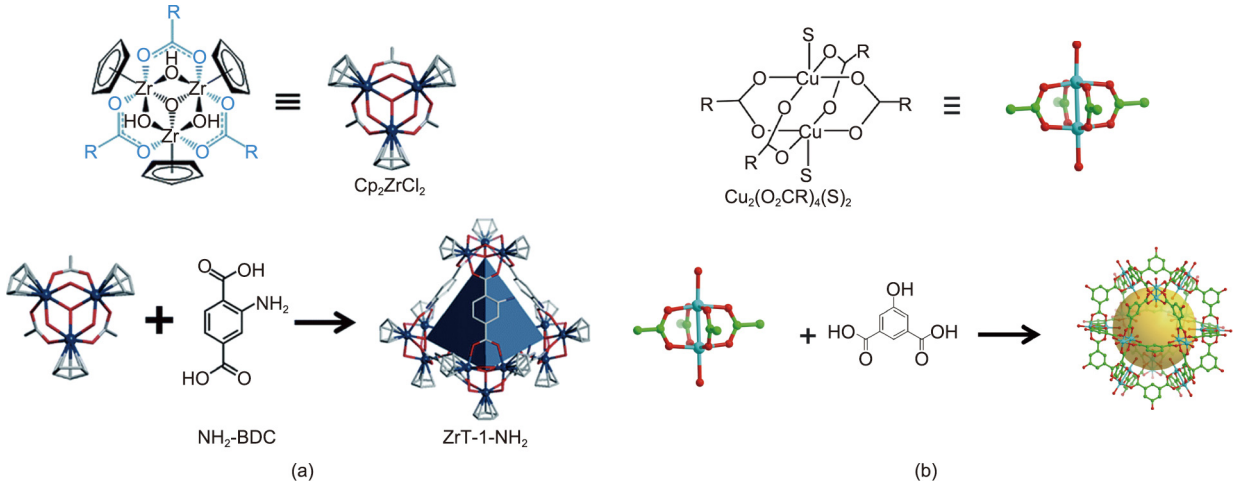

Fig. 4. (a) Crystal structure of the amino-functionalized Zr-MOC (ZrT-1-NH_2) formed by 2-aminoterephthalic acid (NH_2-BDC) and Cp_2ZrCl_2; (b) crystal structure of the hydroxyl-functionalized Cu-MOC formed by 5-hydroxyisophthalic acid and dinuclear Cu(II) paddlewheel units. (a) Reproduced from Ref. [68] with permission.

3.1. Conventional MMMs

3.1.1. MOF-based conventional MMMs

The physical mixing of MOFs with polymers is a versatile and efficient way to fabricate MMMs without the need for complicated reactions and fabrication processes. To achieve better dispersion of MOFs within the polymeric matrix and, accordingly, good separation performance, researchers usually focus on regulating MOF geometry and MOF functionality. Downsizing the MOF particle size to several tens of nanometers is beneficial to improve MOF particle dispersity [89,90]. For example, nano-sized UiO-66 (20–30 nm) exhibited improved dispersion in a polymer of intrinsic microporosity (PIM-1) matrix, resulting in a 40% increase in CO_2/N_2 selectivity [91]. Large agglomerates of nano-sized UiO-66 were not observed within the PIM-1 matrix, in contrast to micro-sized UiO-66-based MMMs. Nano-sized ZIF-67 (25–35 nm) was also prepared and incorporated into a PIM-1 matrix to fabricate MMMs with a 69% increase in CO_2/CH_4 selectivity, while micro-sized ZIF-67-based MMMs only exhibited a 35% increase of selectivity [92]. Recently, He et al. [93] synthesized nano-sized ZIF-8 (~100 nm) in a PIM-1 matrix using *in situ* methods. Due to excellent interfacial compatibility, massive MOF loadings of up to 67.2 wt% were achieved. These ultrahigh MOF loadings effectively enhanced the CO_2 solubility, as confirmed by complementary density functional theory (DFT) simulation, which was quite different from other published results in which MOFs generally promoted gas diffusion.

In addition to particle size, MOF morphology affects the separation performance of MMMs. For example, compared with a pristine Matrimid 5218 membrane, MIL-53 nanoparticle-based MMMs exhibited an improved CO_2 permeability from 8.01 to 9.03 Barrer (1 Barrer = 3.35×10^{-16} mol·m·$(m^2 \cdot s \cdot Pa)^{-1}$), while MIL-53 nanorod- and MIL-53 microneedle-based MMMs exhibited a decreased CO_2 permeability of 7.52 Barrer [56]. The researchers indicated that these results might be due to better disruption of the polymer chains by the MIL-53 nanoparticles, producing more free volume in the polymeric matrix [56]. ZIF-8 with five different shapes was synthesized and incorporated into a polyethylene oxide (PEO) matrix to fabricate MMMs [94]. Gas permeability measurements showed that nanorod ZIF-8-based MMMs exhibited the best performance for C_3H_6/C_3H_8 separation (permeability P_{C3H6} = 16.6 Barrer, separation selectivity $\alpha_{C3H6/C3H8}$ = 9.2), probably due to the intensification of the molecular-sieving effect of the nanorod ZIF-8 framework [94]. MOFs with hollow interior structures are preferred in order to minimize the transport resistance of gas through the core of the fillers, while their molecular-sieving shells afford high selectivity. For example, ZIF-67/PIM-1 MMMs with hollow ZIF-67 particles exhibited an improved CO_2 permeability of 37%, compared with ZIF-67/PIM-1 MMMs with solid ZIF-67 particles [95].

MOF functionalization is a popular way to engineer the MOF–polymer interface. The construction of MOFs with rich functional groups (e.g., $-NH_2$, –OH, –CN) via direct assembly or PAM is useful for fabricating high-performance MMMs and has been investigated extensively in the past decade [91,96–103]. Recently, Jiang et al. [104] prepared an imidazole-2-carboxyaldehyde-functionalized UiO-66-NH_2 (i.e., UiO-66-NH_2@ICA) via PAM. Compared with pristine UiO-66-NH_2, the as-synthesized UiO-66-NH_2@ICA showed a higher CO_2 adsorption capacity due to the increased density of the CO_2-philic nitrogen (N) atoms decorating the pore environment. Accordingly, the as-fabricated UiO-66-NH_2@ICA/Matrimid 5218 MMM with 10 wt% of filler loading exhibited 40% increased CO_2/CH_4 selectivity compared with the UiO-66-NH_2/Matrimid 5218 MMM. A novel "delayed linker addition" protocol was proposed by Hillman et al. [105] to prepare a hybrid ZIF-8 framework containing unsubstituted imidazolate linkers. The as-fabricated MMMs exhibited excellent C_3H_6 permeability (P_{C3H6} = 111.9 Barrer) and C_3H_6/C_3H_8 separation selectivity ($\alpha_{C3H6/C3H8}$ = 14.3) [105]. Molecular simulations further revealed that the improved permeability with increasing unsubstituted imidazolate linkers was due to the increasing number of larger and more flexible apertures within the hybrid ZIF-8 framework.

The functionalization of MOF surfaces with a second porous filler in order to construct core–shell composite structures can tune the surface characteristics of MOFs with increased surface roughness, surface area, or affinity to the surrounding polymeric matrix [106,107]. Due to the wholly organic nature of COFs, Cheng et al. [108] prepared a MOF@COF core–shell filler (i.e., UiO-66-NH_2@TpPa-1) by means of a two-step polymerization and crystallization process, in which the COF outer layers efficiently avoided the formation of nonselective voids (Fig. 5). The as-fabricated UiO-66-NH_2@TpPa-1/polysulfone (PSf) MMM with 5 wt% of filler loading exhibited a CO_2/CH_4 selectivity of 46.7, which was significantly greater than that of the pristine PSf membrane and the UiO-66-NH_2/PSf MMM. MOF@MOF core–shell fillers have also been prepared and introduced into a polymeric matrix for MMM fabrication. Song et al. [107] utilized a layer-by-layer deposition method to prepare a UiO-66-NH_2@ZIF-8 core–shell filler. Compared with the UiO-66-NH_2/PSf MMM, the CO_2/N_2 selectivity of the as-fabricated UiO-66-NH_2@ZIF-8/PSf MMM increased to 39 due to the smaller pore size of the ZIF-8 shell, which enhanced the molecular sieving of the core–shell filler [107]. Other types of MOF@MOF core–shell fillers have also been successfully synthesized using ZIFs as a shell [109–111]. Recently, Wu et al. [112] reported the growth of a sub-20 nm uneven MOF-74 shell on a MOF surface (e.g., MOF-808, UiO-66, UiO-66-NH_2) (Fig. 6). Compared with the pristine 4,4′-(hexafluoroisopropylidene)diphthalic anhydride (6FDA)–durene membrane, the ethylene/ethane (C_2H_4/C_2H_6) selectivity of the as-fabricated MOF-801@MOF-74/6FDA–durene MMM dramatically increased to 5.91, surpassing the 2013 Robeson upper bound. This outstanding separation performance stemmed from the high-density open metal sites on the MOF-74 shell, which allowed the filler to coordinatively crosslink with the polymeric matrix, thereby ensuring good interfacial compatibility and enhanced C_2H_4/C_2H_6 selectivity [112]. A molecular dynamics simulation was carried out to characterize the interactions between MOF-74 and 6FDA–durene polymer. Subsequently, the researchers utilized similar chemistry to construct a MOF@nanocapsule core–shell filler, in which the open metal sites on the nanocapsule (i.e., PgC_5Cu) coordinatively crosslinked with the polar functional groups on polymers, including PSf, PIM, and polyimide (PI), achieving improved dispersity [113].

MOF functionalization by means of macromolecules is another popular and efficient method for improving interfacial compatibility and separation performance. This is because the polymer nature of macromolecules presents the possibility of filling the gaps between the porous fillers and polymeric matrix. For example, ZIF-8 was coated with a polydopamine (PDA) layer to obtain ZIF-8@PDA nanoparticles [114]. The formation of hydrogen bonds between ZIF-8@PDA and the PI matrix helped eliminate undesirable interfacial voids and enhance the gas separation selectivity of the MMMs while slightly sacrificing permeability. Directly grafting identical macromolecules that match the polymeric matrix is beneficial for engineering the interfacial interaction. For example, Wang et al. [115] reported the grafting of polyvinylamine (PVAm) on a MIL-101(Cr) surface. Improved interfacial compatibility was observed between the PVAm-modified MIL-101(Cr) particles and the PVAm matrix due to the formation of hydrogen bonds, which were also helpful for the fabrication of a defect-free ultrathin membrane [115]. Using a novel gravity-induced interface self-assembly technique, ultrathin MMMs (thickness: ~200 nm) with unobstructed gas transport channels through the selective layer were successfully fabricated, exhibiting a CO_2 permeance of 823

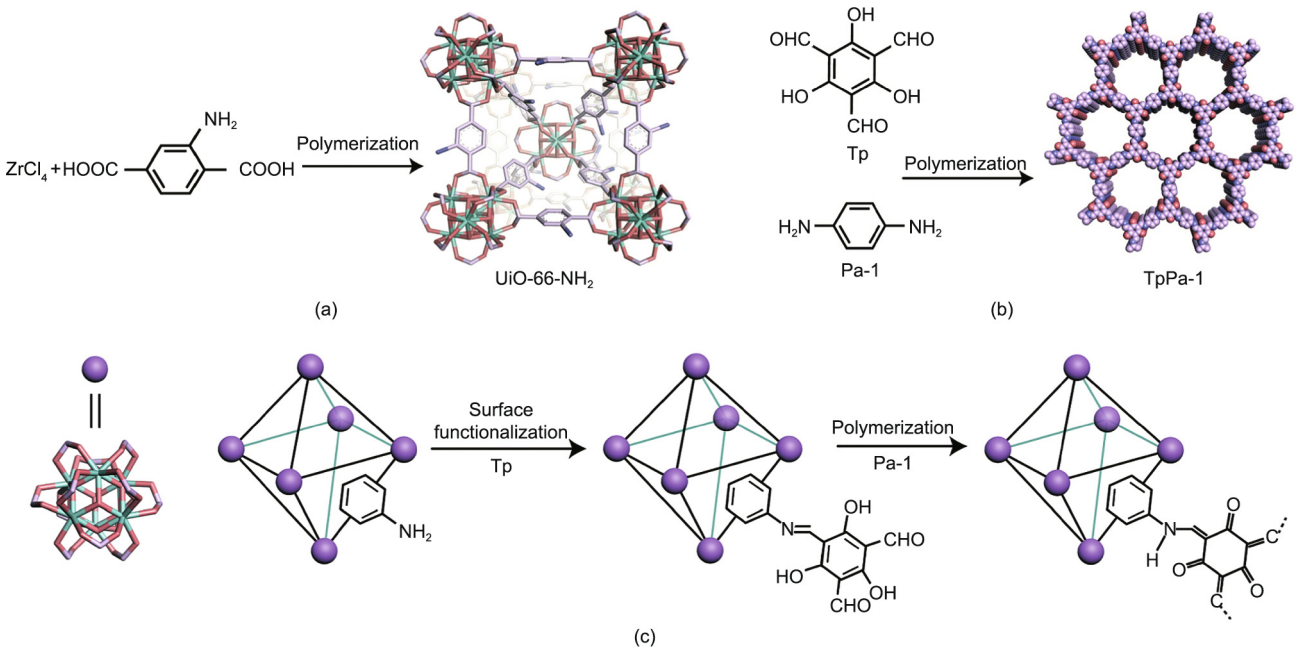

Fig. 5. Synthetic route of (a) UiO-66-NH_2, (b) TpPa-1, and (c) UiO-66-NH_2@TpPa-1 composite filler. Tp: triformylphloroglucinol; Pa-1: *p*-phenylenediamine. Reproduced from Ref. [108] with permission.

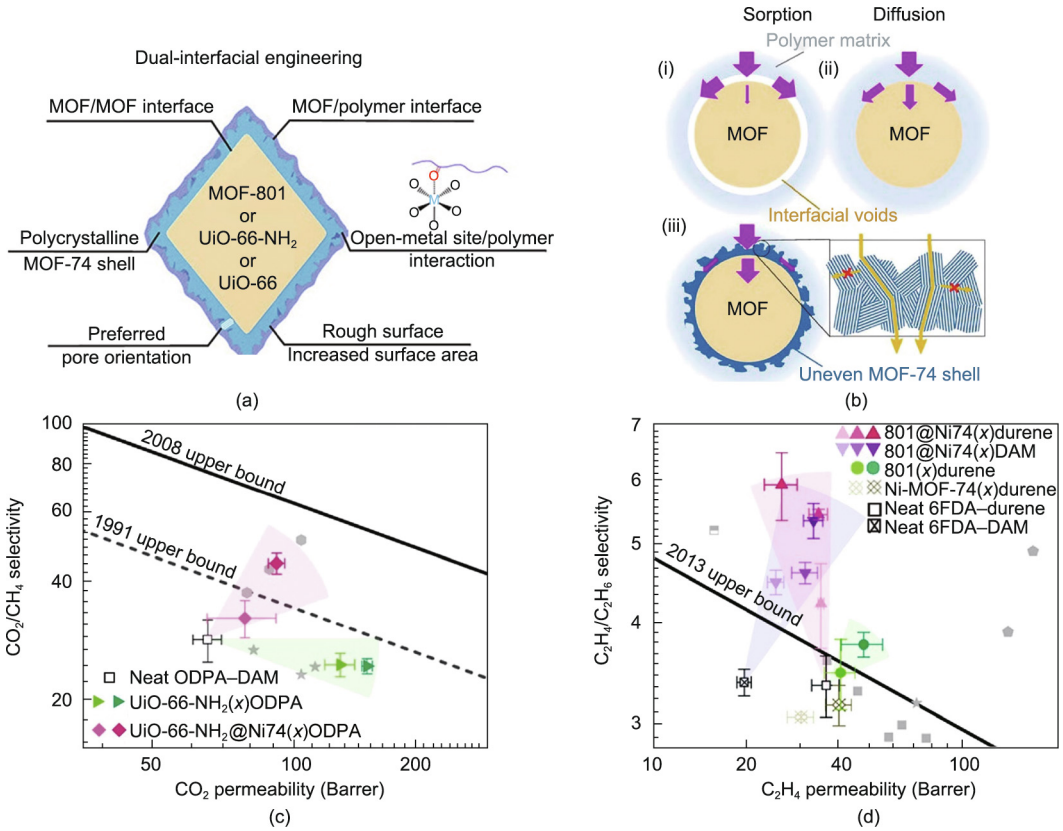

Fig. 6. Schematic diagrams of (a) MOF@MOF-74 composite fillers and (b) gas transport through the pore channels of MOF@MOF-74 composite fillers. (c) CO_2/CH_4 separation performance of pristine ODPA–DAM, UiO-66-NH_2(*x*)ODPA (*x* = 9 and 24), and UiO-66-NH_2@Ni74(*x*)ODPA (*x* = 10 and 22) membranes. (d) C_2H_4/C_2H_6 separation performance of pristine 6FDA–durene, pristine 6FDA–DAM, MOF-801(*x*)durene (*x* = 9 and 22), MOF-801@Ni74(*x*)durene (*x* = 10, 16, and 26), MOF-801@Ni74(*x*)DAM (*x* = 8, 10, and 18), and Ni-MOF-74(*x*)durene (*x* = 2.4 and 18) membranes. The *x* in parentheses represents the weight percentages of the fillers in the MMMs. For each membrane, the light to dark symbol colors represent low to high filler loadings in the membrane, respectively. ODPA: 4,4′-oxidiphthalic anhydride; DAM: 2,4,6-trimethyl-1,3-phenylenediamine; 6FDA: 4,4′-(hexafluoroisopropylidene)diphthalic anhydride. Reproduced from Ref. [112] with permission.

gas permeation units (GPU) and a CO_2/N_2 separation selectivity of 242. By using PI as a matrix, 4,4′-oxidiphthalic anhydride (ODPA)–2,4,6-trimethyl-1,3-phenylenediamine (DAM) PI oligomers were covalently grafted onto a UiO-66-NH_2 surface to enhance MOF dispersity in the PI matrix [116]. The resulting MMMs showed excellent CO_2/CH_4 and CO_2/N_2 separation performance (P_{CO2} = 142 Barrer, $\alpha_{CO2/CH4}$ = 43, $\alpha_{CO2/N2}$ = 27) and improved CO_2 plasticization resistance (Fig. 7) [116]. Similar strategies have also been adopted by Qian et al. [117] and Dai et al. [118] to covalently graft PI oligomers onto the surface of UiO-66-NH_2 and MIL-101(Cr), respectively.

Polyethyleneimine (PEI), which has rich –NH_2 groups on its backbone, is considered to be a good modifying agent for tuning MOF surface properties and interfacial compatibility. Xin et al. [57] utilized a vacuum-assisted method to prepare PEI-functionalized MIL-101(Cr), in which PEI brushes were attached to the internal and external surfaces of MIL-101(Cr) particles. Electrostatic interactions and hydrogen bonds formed between the –SO_3H group on the sulfonated poly(ether ether ketone) (SPEEK) matrix and the –NH_2 group on the PEI brushes [57]. Accordingly, the as-fabricated MIL-101(Cr)@PEI/SPEEK MMM exhibited a 128.1% enhanced CO_2/CH_4 selectivity in comparison with the MIL-101(Cr)/SPEEK MMM. Using glutaraldehyde as a covalent cross-linker, PEI brushes have also been applied to graft on a Christian-Albrecht University (CAU)-1 surface [119]. Recently, Wang et al. [120] revealed the potential of grafting polymer brushes with various configurations in order to affect the membrane separation performance (Fig. 8). The grafting of branched PEI is helpful in enhancing the membrane selectivity, while the grafting of block copolymer polyether block amide (Pebax) is conducive to increasing the membrane permeance [120]. Other types of macromolecules, such as PEG, poly(ionic liquid), and poly(dimethylsiloxane) (PDMS), have also been adopted to functionalize MOF surfaces, resulting in improved interfacial compatibility and separation performance [121–123]. The gas separation performance of MOF-based conventional MMMs in recent studies is summarized in Table 1 [45,56,57,91–95,104,105,107,108,112,114–120,124].

3.1.2. MOC-based conventional MMMs

Although the use of MOCs in MMMs is relatively new, MOCs are promising in demonstrating similar properties to MOFs in MMM fabrication. In particular, the solubility and processibility of MOCs enable them to be integrated into industrial membrane fabrication processes. In contrast to MOF particles, which form suspensions in solvent media, MOCs act as discrete molecules and disperse uniformly within a polymeric matrix at the molecular level. A key step in the fabrication of MOC-based MMMs is to match the solubility of the MOCs with that of the selected polymer. In this respect, Cu-MOCs have been greatly investigated for the fabrication of MOC-based MMMs due to their suitable pore size, easy functionality, and good solubility in common solvents.

By using PI as a matrix, a –NH_2 functionalized Cu-MOC (i.e., MOP-15) was dissolved in dimethyl sulfoxide (DMSO) and then incorporated into a 6FDA–DAM PI matrix during MMM fabrication [125]. In contrast to MOF-based MMMs, which usually attain optimal performance at filler loadings of 10–20 wt%, the addition of just 1.6 wt% of MOC resulted in a 40% improvement in CO_2 permeability, with good aging resistance. However, further increasing the MOC loading to 7.4 wt% led to a dramatically decreased selectivity

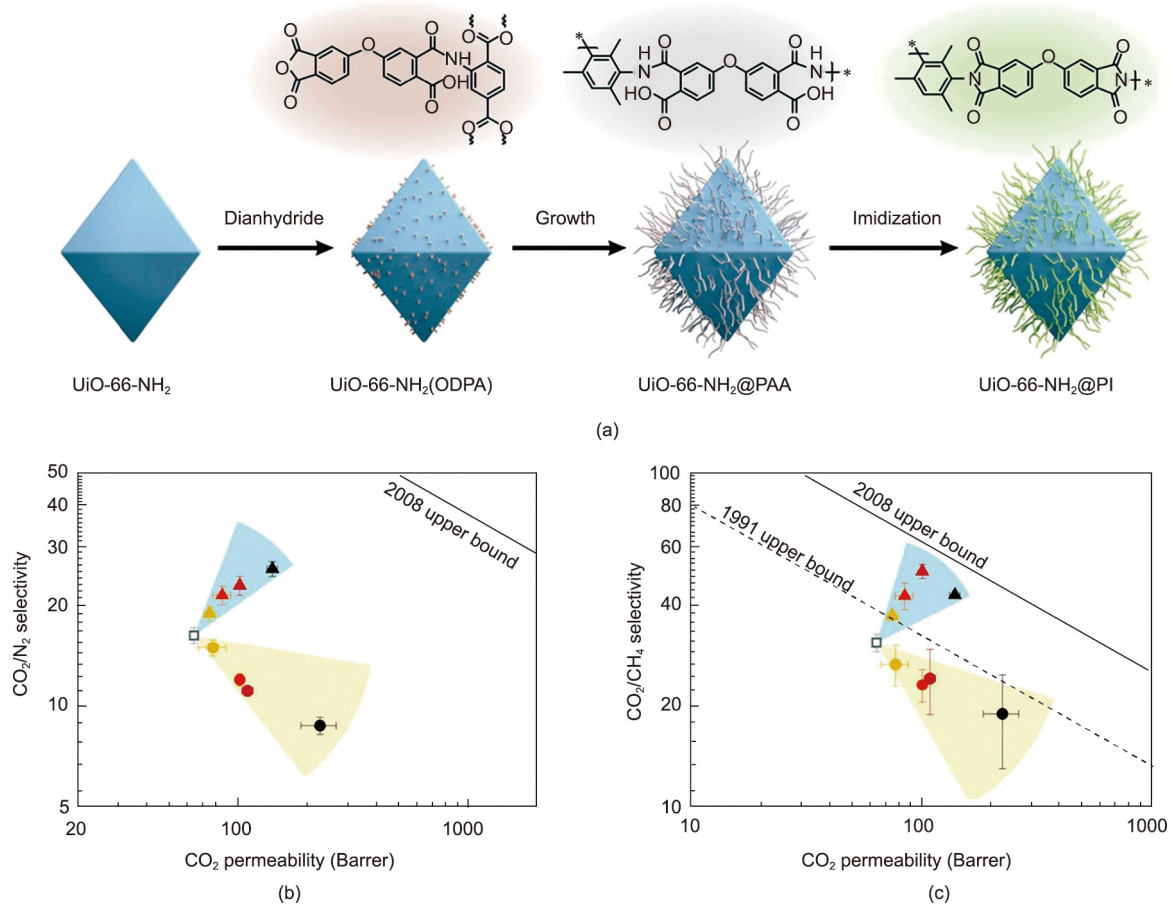

Fig. 7. (a) Synthetic route of UiO-66-NH_2@PI. (b) CO_2/N_2 and (c) CO_2/CH_4 separation performance of the pristine PI (opened square), UiO-66-NH_2@PI/ODPA–DAM MMM (closed triangle), and UiO-66-NH_2/ODPA–DAM MMM (closed circle) with different loadings of 5% (yellow symbols), 9% (orange symbols), 17% (red symbols), or 27% (black symbols). Reproduced from Ref. [116] with permission.

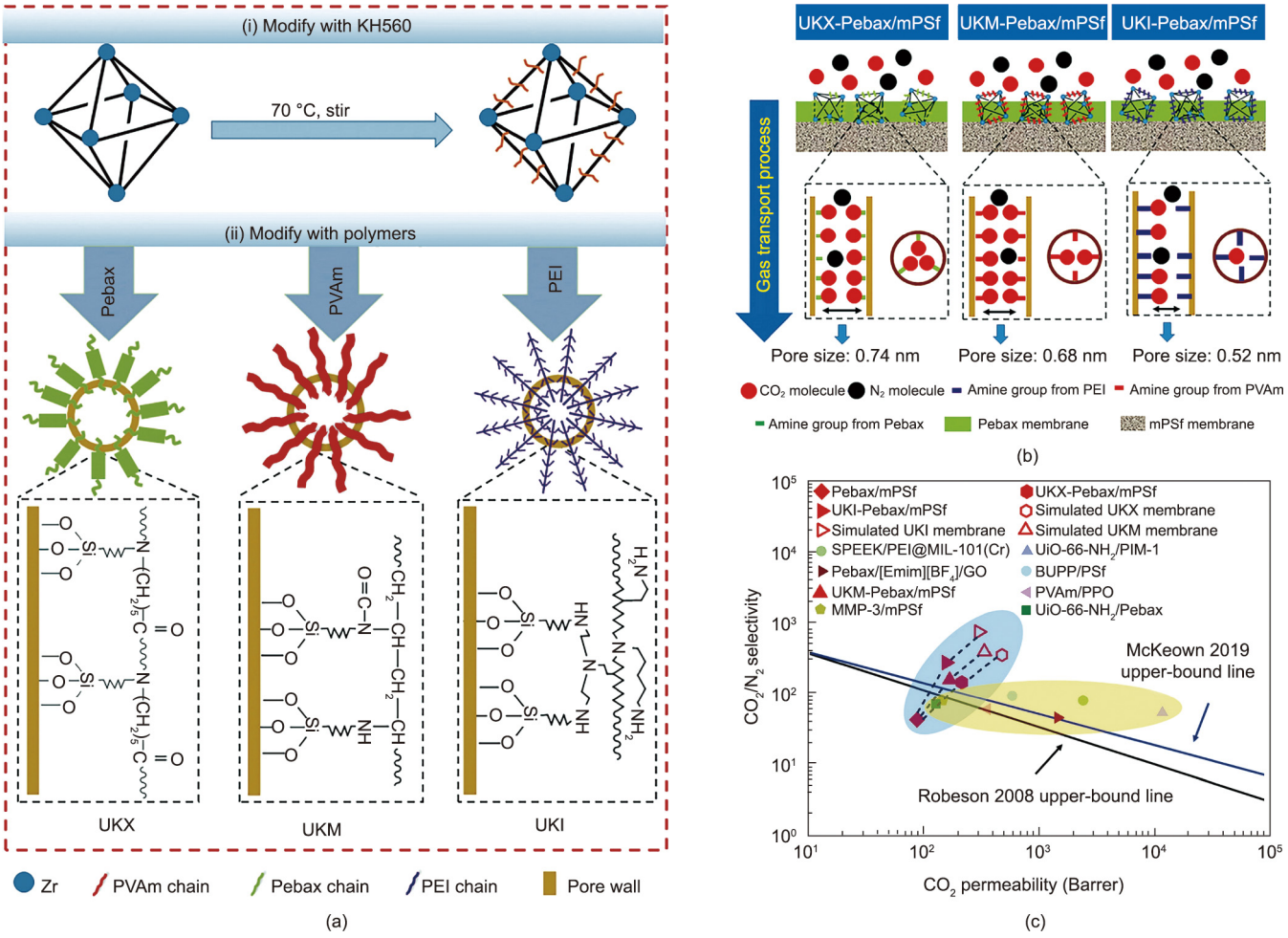

Fig. 8. (a) Synthetic route of Pebax-, PVAm-, and PEI-functionalized UiO-66; (b) schematic diagram of gas transport through the pore channels of Pebax-, PVAm-, and PEI-functionalized UiO-66; (c) CO_2/N_2 separation performance of the fabricated MMMs. UKX, UKM, and UKI were species that synthesized via post-modification of UiO-66 by Pebax, PVAm, and PEI, respectively. KH560: 3-glycidyloxypropyltrimethoxysilane; mPSf: modified polysulfone; PPO: poly(phenylene oxide); MMP: metal-induced ordered microporous polymer; [Emim][BF_4]: 1-ethyl-3 methylimidazolium tetrafluoroborate; GO: graphene oxide; BUPP: bridging UiO-66-NH_2-poly(ethylene glycol) diglycidyl ether (PEGDE)-PVAm. Reproduced from Ref. [120] with permission.

Table 1
Summary of the gas separation performance of MOF-based conventional MMMs.

Polymer	Filler	Operation condition	Gas pair	Separation performance	Ref.
XLPEO	ZIF-7-NH_2	0.5 MPa, 35 °C, mixed gas	CO_2/CH_4	P_{CO2} = 215 Barrer, $\alpha_{CO2/CH4}$ = 55	[45]
XLPEO	CAU-1-PEI	0.3 MPa, 35 °C, mixed gas	CO_2/CH_4	P_{CO2} = 546 Barrer, $\alpha_{CO2/CH4}$ = 27.8	[119]
PIM-1	Nano-sized UiO-66	0.4 MPa, 25 °C, single gas	CO_2/CH_4, CO_2/N_2	P_{CO2} = 2869 Barrer, $\alpha_{CO2/CH4}$ = 28.3, $\alpha_{CO2/N2}$ = 27.5	[91]
PIM-1	Nano-sized ZIF-67	0.2 MPa, 30 °C, mixed gas	CO_2/CH_4	P_{CO2} = 2567 Barrer, $\alpha_{CO2/CH4}$ = 19.8	[92]
6FDA–DAM	MIL-53 nanoparticle	0.3 MPa, 25 °C, mixed gas	CO_2/CH_4	P_{CO2} = 660 Barrer, $\alpha_{CO2/CH4}$ = 28	[56]
XLPEO	ZIF-8 nanorod	35 °C, mixed gas	C_3H_6/C_3H_8	P_{C3H6} = 16.6 Barrer, $\alpha_{C3H6/C3H8}$ = 9.2	[94]
PIM-1	Hollow ZIF-67	0.2 MPa, 30 °C, mixed gas	CO_2/CH_4	P_{CO2} = 7128 Barrer, $\alpha_{CO2/CH4}$ = 16.4	[95]
Matrimid 5218	UiO-66-NH_2@ICA	0.3 MPa, 25 °C, mixed gas	CO_2/CH_4	P_{CO2} = 40.1 Barrer, $\alpha_{CO2/CH4}$ = 64.7	[104]
PSf	UiO-66-NH_2@TpPa-1	0.1 MPa, 25 °C, mixed gas	CO_2/CH_4	P_{CO2} = 7.1 Barrer, $\alpha_{CO2/CH4}$ = 46.7	[108]
PSf	UiO-66-NH_2@ZIF-8	0.3 MPa, 35 °C, single gas	CO_2/N_2	P_{CO2} = 45.2 Barrer, $\alpha_{CO2/N2}$ = 39	[107]
6FDA–durene	MOF-801@MOF-74	0.3 MPa, 35 °C, single gas	C_2H_4/C_2H_6	P_{C2H4} = 26 Barrer, $\alpha_{C2H4/C2H6}$ = 5.91	[112]
TBDA2–6FDA	ZIF-8@PDA	0.1 MPa, 35 °C, single gas	H_2/CH_4, H_2/N_2	P_{H2} = 1858 Barrer, $\alpha_{H2/CH4}$ = 36, $\alpha_{H2/N2}$ = 27	[114]
PVAm	MIL-101(Cr)-PVAm	0.5 MPa, 25 °C, mixed gas	CO_2/N_2	P_{CO2} = 823 GPU, $\alpha_{CO2/N2}$ = 242	[115]
ODPA–DAM	UiO-66-NH_2@PI	0.31 MPa, 35 °C, single gas	CO_2/CH_4, CO_2/N_2	P_{CO2} = 142 Barrer, $\alpha_{CO2/CH4}$ = 43, $\alpha_{CO2/N2}$ = 27	[116]
6FDA–durene	UiO-66-NH_2@PI	0.1 MPa, 35 °C, single gas	CO_2/CH_4	P_{CO2} = 1890 Barrer, $\alpha_{CO2/CH4}$ = 18	[117]
6FDA–DDS	NH_2-PIEM⊂MIL-101(Cr)@PI	0.3 MPa, 35 °C, single gas	CO_2/CH_4, CO_2/N_2	P_{CO2} = 54.8 Barrer, $\alpha_{CO2/CH4}$ = 61.1, $\alpha_{CO2/N2}$ = 32.5	[118]
Sulfonated SPEEK	MIL-101(Cr)@PEI	0.1 MPa, 25 °C, single gas	CO_2/CH_4, CO_2/N_2	P_{CO2} = 2490 Barrer, $\alpha_{CO2/CH4}$ = 71.8, $\alpha_{CO2/N2}$ = 80	[57]
Pebax/mPSf	UiO-66@PEI	0.15 MPa, 35 °C, mixed gas	CO_2/N_2	P_{CO2} = 1120 GPU, $\alpha_{CO2/N2}$ = 278	[120]
Pebax/mPSf	UiO-66@Pebax	0.15 MPa, 35 °C, mixed gas	CO_2/N_2	P_{CO2} = 1683 GPU, $\alpha_{CO2/N2}$ = 146	[120]
6FDA–DAM	Defective UiO-66	0.2 MPa, 35 °C, single gas	C_3H_6/C_3H_8	P_{C3H6} = 237 Barrer, $\alpha_{C3H6/C3H8}$ = 9.8	[124]
6FDA–DAM	Im/ZIF-8	0.1 MPa, 25 °C, single gas	C_3H_6/C_3H_8	P_{C3H6} = 111.9 Barrer, $\alpha_{C3H6/C3H8}$ = 14.3	[105]
PIM-1	Nano-sized ZIF-8	0.35 MPa, 35 °C, single gas	CO_2/CH_4, CO_2/N_2	P_{CO2} = 6338 Barrer, $\alpha_{CO2/CH4}$ = 18.8, $\alpha_{CO2/N2}$ = 24.4	[93]

XLPEO: crosslinked poly(ethylene oxide); TBDA2: 3,9-diamino-4,10-dimethyl-6,12-dihydro-5,11-methanodibenzo[*b*,*f*][1,5]diazocine; DDS: 4,4′-diaminodiphenyl sulfone; ICA: imidazolate-2-carboxyaldehyde; PIEM: poly(isocyanatoethyl methacrylate).

due to the aggregation of MOCs at this loading. Focused ion beam scanning electron microscopy (FIB-SEM) further provided visualization of the MOC dispersion within the polymeric matrix. At a loading of 1.6 wt%, a homogeneous membrane with discrete MOC molecules (2–3 nm) embedded in the matrix could be clearly observed. To enhance the solubility of MOCs in commonly used low-boiling-point solvents, an alkyl chain-decorated Cu-MOC (i.e., MOP-18), which is highly soluble in chloroform ($CHCl_3$), was incorporated into a Matrimid 5218 matrix for MMM fabrication [65]. Scanning electron microscopy (SEM) revealed that the MOP-18 did not aggregate within the matrix even at loadings as high as 80 wt%, which is quite distinct from MOF-based MMMs.

The incorporation of Cu-MOC has also been found to improve the anti-aging property of poly(1-trimethylsilyl-1)propyne (PTMSP) membranes, which have been known to be susceptible to such phenomena (Fig. 9) [126]. By comparing the anti-aging property of MMMs constructed using four types of Cu-MOCs (i.e., *tert*-butyl (^{t}Bu) MOP, diethylene glycol (DEG) MOP, triethylene glycol (TEG) MOP, and MOP-18) with different lengths of non-polar hydrocarbons or polar PEG chains on the ligand, the researchers concluded that the anti-aging property of the MMMs was mainly caused by the length—rather than the chemistry—of the MOC side chain [126].

PEO, a highly CO_2-philic polymer, has also been applied as a matrix to fabricate MOC-based MMMs. Cu-MOC with polar $–SO_3Na$ groups on its side chain (i.e., MOP-3) was incorporated into a PEO matrix for CO_2 separation [127]. Increasing the Cu-MOC loading was found to increase the CO_2 permeability of the MMMs, although a slightly decreased selectivity was observed. Unlike the fabrication of dense MMMs, Sohail et al. [128] prepared ultrathin MOC-based MMMs via an atom transfer radical polymerization (ATRP)-based continuous assembly of polymers (CAP) technique. The presence of unsaturated metal sites and PEG chains on Cu-MOC facilitated CO_2 transport within the PEO matrix, resulting in enhanced CO_2 solubility and CO_2 solubility selectivity, as confirmed by sorption analysis (Fig. 10) [128]. Accordingly, the ultrathin MMMs exhibited a high CO_2 permeance of 448 GPU and a high CO_2/N_2 selectivity of 30. The thickness of the membrane was around 291 nm, and the thickness of the selective layer could be controlled to be less than 50 nm, highlighting the significance of the ATRP-based CAP technique for ultrathin MMM fabrication. MOCs with other topologies or metals have also been incorporated into polymeric matrixes for efficient gas separation [129]. The gas separation performance of MOC-based conventional MMMs in recent studies is summarized in Table 2 [65,125,127–130].

3.2. Covalently bonded MMMs

3.2.1. MOF-based covalently bonded MMMs

Covalently bonding MOFs with polymers via facile reactions is considered to be a powerful method to reinforce the interfacial interactions in order to achieve defect-free membranes. PI and PIM are commonly studied glassy polymers used to form covalent linkages with MOFs. Yu et al. [101] reported the chemical crosslinking of PIM-1 and UiO-66-CN to fabricate UiO-66-CN@sPIM-1 MMMs via the thermal rearrangement of PIM-1 (sPIM-1) (Fig. 11). The as-fabricated MMMs showed a high CO_2 permeability of 12 063 Barrer and a CO_2/N_2 selectivity of 53.5. The fluoride on PIM-1 can also react with the –OH group on Mg-MOF-74, forming an inter-connected micropore network [131]. Accordingly, Mg-MOF-74@PIM-1 MMM exhibited a simultaneous improvement of CO_2 permeability to 21 269 Barrer and CO_2/CH_4 selectivity to 19.1 [131]. $[Cd_2L(H_2O)]_2{\cdot}5H_2O$ (Cd-6F) MOF, synthesized with a 6FDA ligand, was incorporated into a 6FDA–oxydianiline (ODA) PI matrix for MMM fabrication via *in situ* polymerization [132]. Improved interfacial compatibility and better separation performance were observed due to the interaction between the uncoordinated $–COO^-$ group on Cd-6F and the $–NH_2$ group on the 6FDA–ODA matrix.

Regarding MMM fabrication with rubbery polymers, Xu et al. [133] fabricated ultrathin MMMs by chemically crosslinking functionalized UiO-66-NH_2 with a PVAm matrix. UiO-66-NH_2 was first modified with poly(ethylene glycol) diglycidyl ether (PEGDE) to obtain epoxy-group-terminated MOF particles (i.e., PEG-UiO-66-NH_2), which were further covalently bonded with a PVAm matrix via a facile epoxide–amine reaction (Fig. 12). The as-fabricated

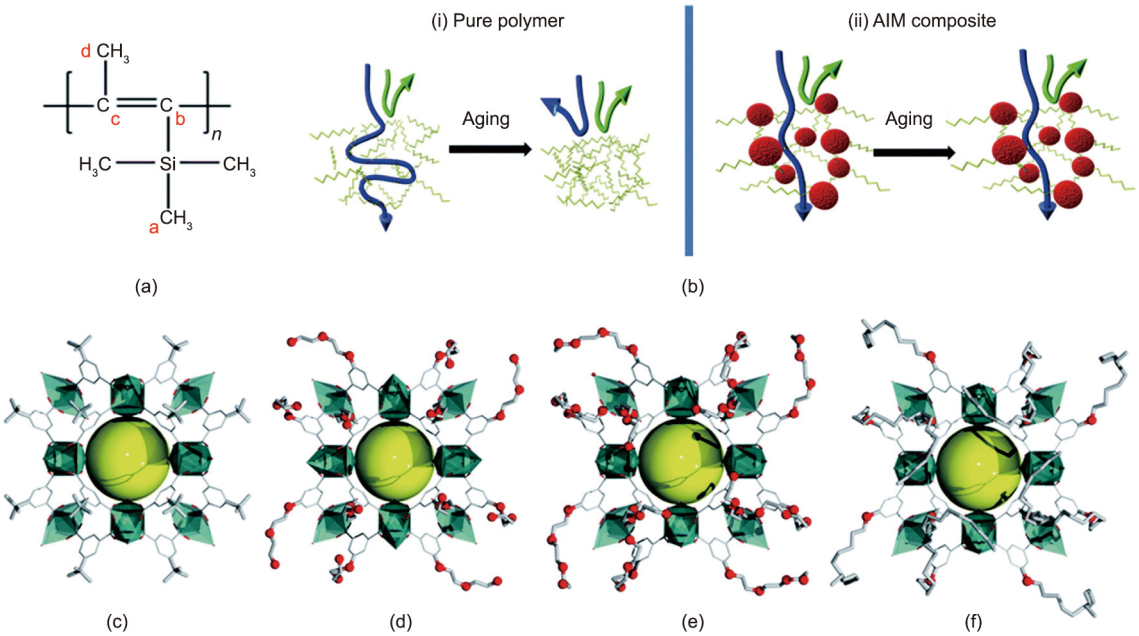

Fig. 9. (a) Structure of the PTMSP matrix; (b) schematic diagram of the pristine PTMSP membrane and the Cu-MOC-based MMM before and after aging. (c–f) Crystal structures of the selected Cu-MOCs: (c) tert-butyl (^{t}Bu) MOP; (d) diethylene glycol (DEG) MOP; (e) triethylene glycol (TEG) MOP; and (f) MOP-18. AIM: anti-aging intercalated membrane. Reproduced from Ref. [126] with permission.

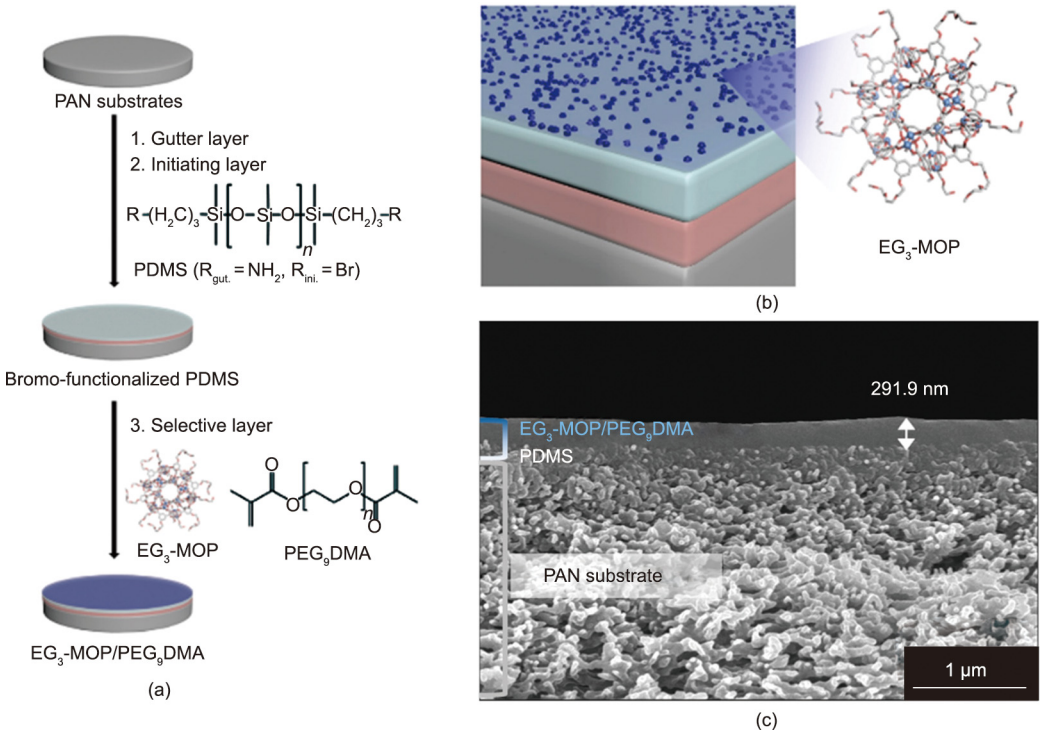

Fig. 10. (a) Synthetic route, (b) schematic diagram, and (c) cross-sectional SEM image of the fabricated EG_3-MOP/PEG_9DMA/PDMS thin film composite MMM. PAN: polyacrylonitrile; EG_3-MOP: triethylene oxide-modified metal–organic polyhedral; PEG_9DMA: poly(ethylene glycol)dimethacrylate. Reproduced from Ref. [128] with permission.

Table 2
Summary of the gas separation performance of MOC-based conventional MMMs.

Polymer	Filler	Operation condition	CO_2/CH_4 gas pair		CO_2/N_2 gas pair		Ref.
			P_{CO2}	$\alpha_{CO2/CH4}$	P_{CO2}	$\alpha_{CO2/N2}$	
PSf	MOP-3	0.3 MPa, 25 °C, mixed gas	15.18 Barrer	34.33	—	—	[130]
Matrimid 5218	MOP-18	0.26 MPa, 35 °C, single gas	14 Barrer	21.9	15.6 Barrer	26	[65]
PVDF	PdMOP	35 °C, single gas	2.5 Barrer	19	2.5 Barrer	13	[129]
PVDF	FeMOP	35 °C, single gas	4.5 Barrer	5.6	4.5 Barrer	23	[129]
PolyPDXLA	MOP-3	0.78 MPa, 35 °C, single gas	580 Barrer	20	580 Barrer	62	[127]
XLPEO	MOP-3	0.78 MPa, 35 °C, single gas	480 Barrer	14	480 Barrer	40	[127]
6FDA–DAM	MOP-15	0.1 MPa, 25 °C, mixed gas	—	—	1413 Barrer	26.7	[125]
PEG_9DMA	EG_3-MOP	0.25 MPa, 35 °C, single gas	—	—	448 GPU	30.1	[128]

PVDF: polyvinylidine fluoride; PolyPDXLA: poly(poly(1,3-dioxolane) acrylate).

MMMs, which had a membrane thickness of 410 nm, exhibited a high CO_2 permeance of 1295 GPU and a CO_2/N_2 selectivity of 91, which were better than those of UiO-66-NH_2/PVAm MMM. By using the acrylate group on PEG precursors, crosslinked MMMs were fabricated via the copolymerization of PEG precursors with isopropenyl-functionalized UiO-66 or vinyl-functionalized Beijing University of Chemical Technology (BUCT) MOFs [134,135]. Crosslinked PDMS-based MMMs have also been successfully fabricated. Katayama et al. [136] prepared a modified UiO-66 via the PAM of hydride-terminated PDMS, which was further reacted with a PDMS matrix via a hydrosilylation reaction [136]. A defect-free MMM with 50 wt% of filler loading was obtained and exhibited good mechanical flexibility. Gao et al. [137] modified UiO-66-NH_2 with *cis*-5-norbornene-exo-2,3-dicarboxylic anhydride (ND), which further participated in the ring-opening metathesis polymerization (ROMP) of norbornene for MMM fabrication. The as-fabricated MMM with 20 wt% of filler loading exhibited a significant improvement in mechanical toughness. A similar ROMP strategy was adopted by Hossain et al. [29] to form a covalent linkage between norbornene-modified UiO-66 (i.e., UiO-66-NB) and a PEG/polypropylene glycol (PPG)–PDMS copolymeric matrix (Fig. 13). The as-fabricated MMMs with 3 wt% of filler loading showed a CO_2 permeability of 585 Barrer and a CO_2/N_2 selectivity of 53, approaching the 2019 Robeson upper bound [29]. An outstanding anti-plasticization property (up to 2.53 MPa) and a stable anti-aging property (up to 11 months) were also observed. The gas separation performance of MOF-based covalently bonded MMMs in recent studies is summarized in Table 3 [29,101,131–133,135,137].

3.2.2. MOC-based covalently bonded MMMs

As with MOF-based MMMs, using simple mixing strategies may not be sufficient to avoid MOC aggregation or phase separation during the fabrication of MOC-based MMMs. The judicious design of the intermolecular interactions between MOCs and polymers is conducive to realizing the full potential of MOCs. Although the covalent hybridization of MOCs with polymers has been investigated extensively as a means of constructing MOC/polymer hybrid materials, the fabrication of MOC-based MMMs using covalent bonding has rarely been reported, especially in the field of gas separation [24,60,63,138]. To achieve covalent bonding, MOCs

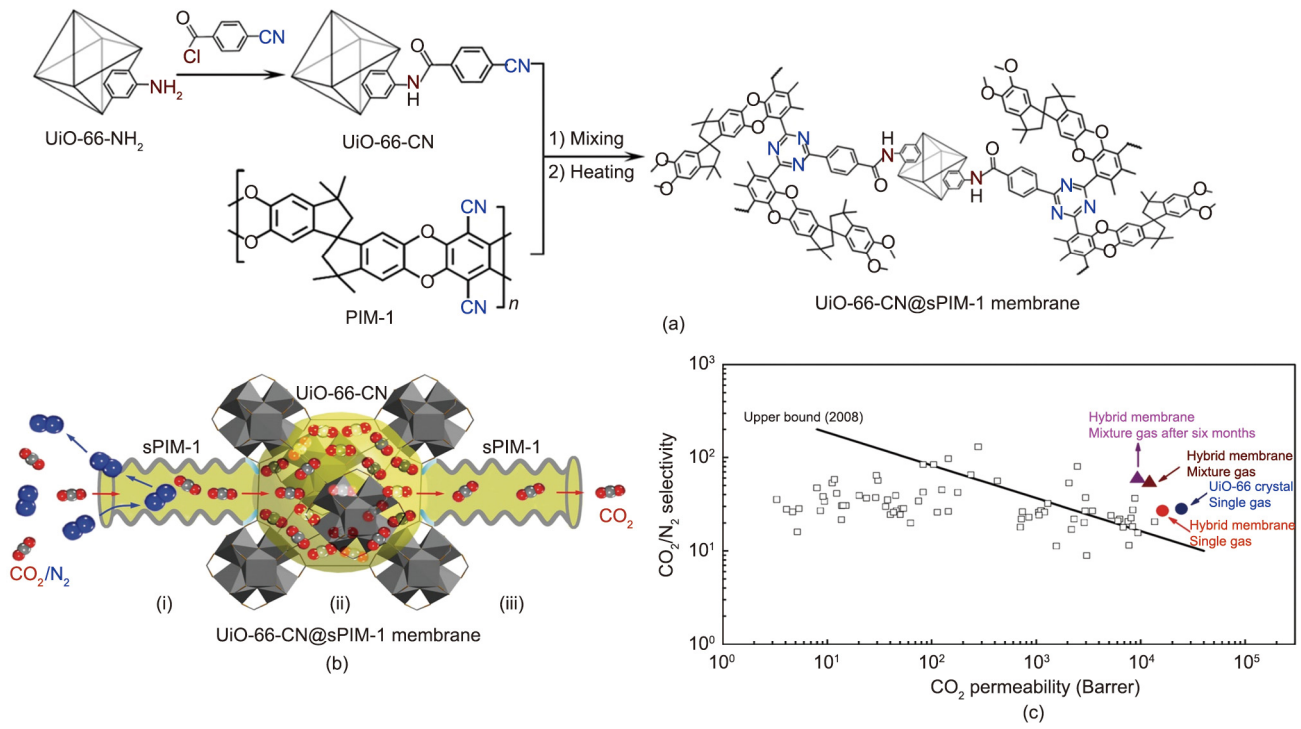

Fig. 11. (a) Synthetic route to fabricate UiO-66-CN@sPIM-1 MMM; (b) schematic diagram of gas transport within UiO-66-CN@sPIM-1 MMM; (c) CO_2/N_2 separation performance of the fabricated UiO-66-CN@sPIM-1 MMM. Reproduced from Ref. [101] with permission.

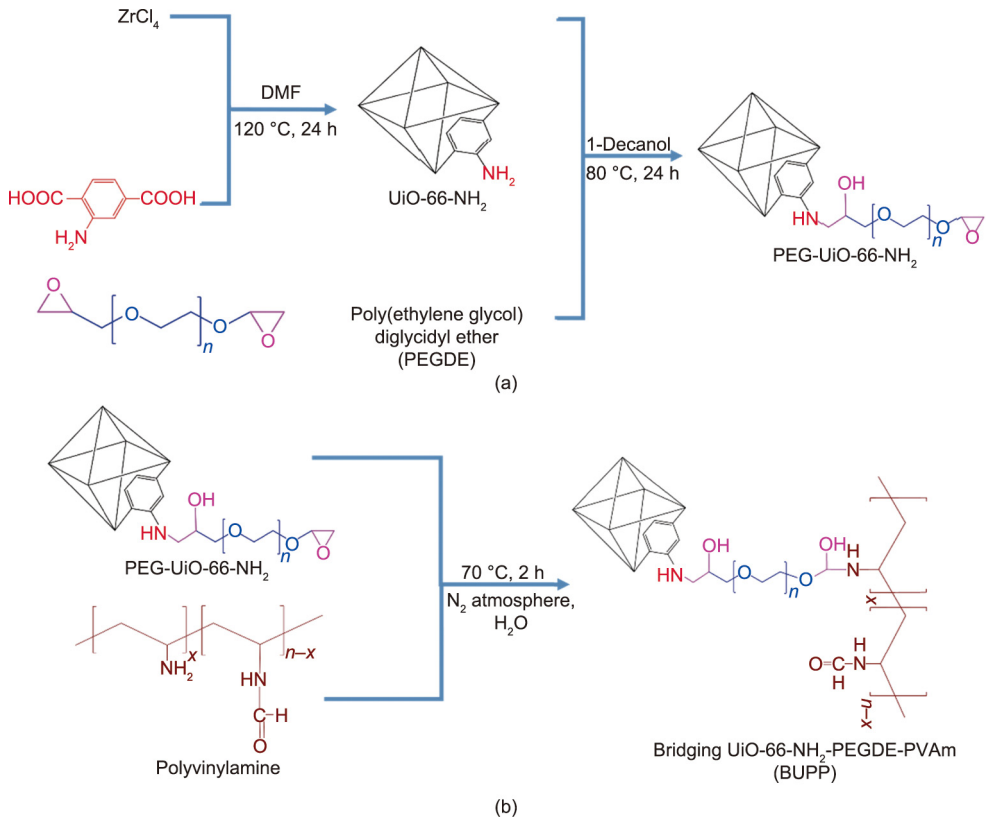

Fig. 12. (a) Synthetic routes of PEG-UiO-66-NH_2 nanoparticles; (b) the fabricated PEG-UiO-66-NH_2/PVAm MMM. Reproduced from Ref. [133] with permission.

must have functional groups that can react with monomers or polymeric precursors for membrane fabrication, along with adequate solubility for subsequent reaction and membrane fabrication processes. Recently, our group reported the fabrication of homoporous hybrid membranes (HHMs) by the chemical crosslinking of a polymerizable Zr-MOC (i.e., ZrT-1-AA) with PEO precursors

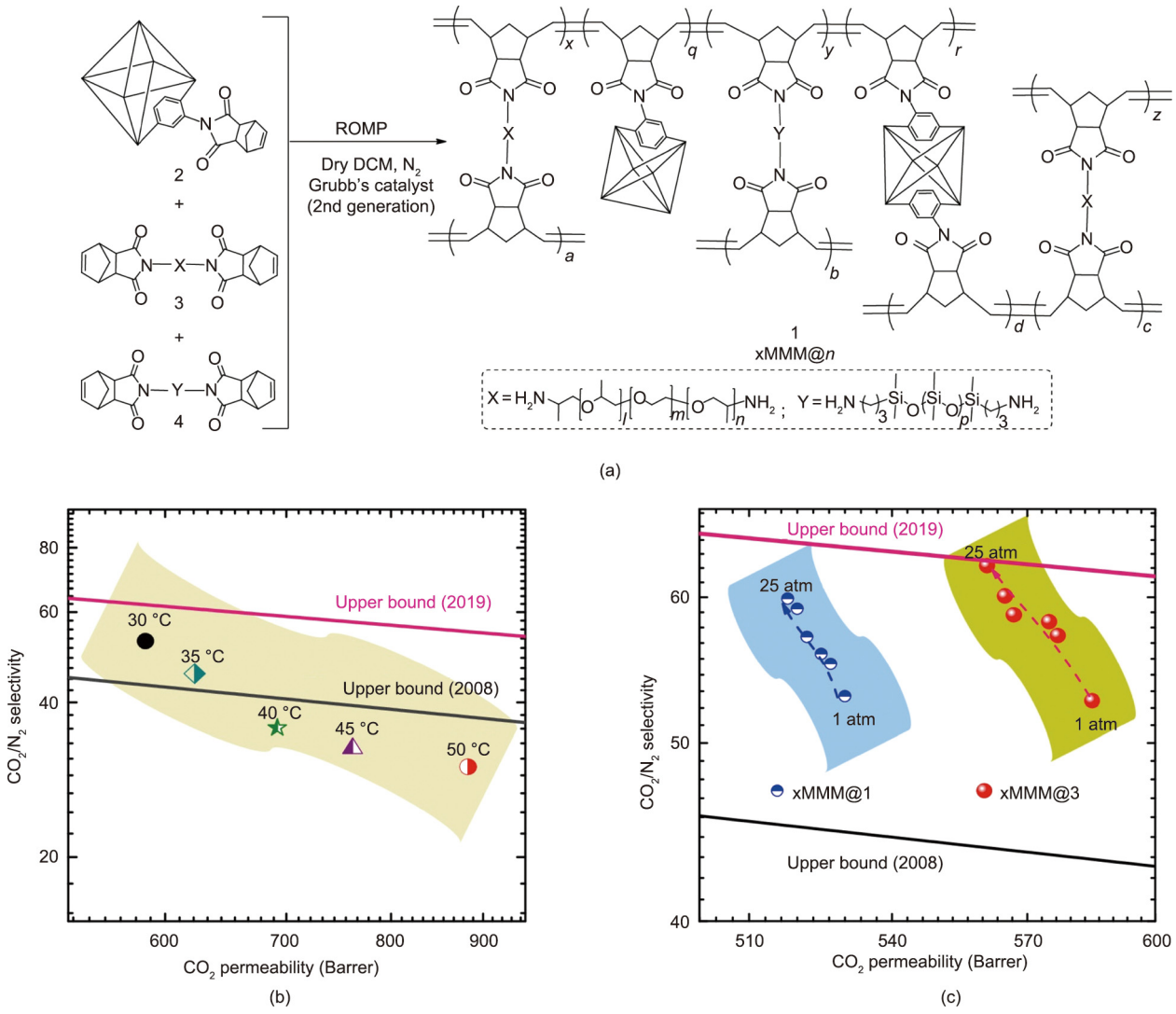

Fig. 13. (a) Synthetic route of the fabricated UiO-66-NB-*n*@x(PEG/PPG–PDMS) MMM. (b, c) CO_2/N_2 separation performance of the fabricated MMMs at different (b) temperatures and (c) pressures (1 atm = 101 325 Pa). xMMM: cross-linked MMM. Reproduced from Ref. [29] with permission.

Table 3
Summary of the gas separation performance of MOF-based covalently bonded MMMs.

Polymer	Filler	Operation condition	Gas pair	Separation performance	Ref.
XLPEO	UiO-66-MA	0.35 MPa, 35 °C, single gas	CO_2/CH_4, CO_2/N_2	P_{CO2} = 1 450 Barrer, $\alpha_{CO2/CH4}$ = 14.2, $\alpha_{CO2/N2}$ = 45.8	[135]
PIM-1	UiO-66-CN	0.14 MPa, 25 °C, mixed gas	CO_2/N_2	P_{CO2} = 12 063 Barrer, $\alpha_{CO2/N2}$ = 53.5	[101]
PIM-1	Mg-MOF-74	0.2 MPa, 25 °C, single gas	CO_2/CH_4	P_{CO2} = 21 269 Barrer, $\alpha_{CO2/CH4}$ = 19.1	[131]
6FDA–ODA	Cd-6F MOF	0.2 MPa, 25 °C, single gas	CO_2/CH_4, CO_2/N_2	P_{CO2} = 37.8 Barrer, $\alpha_{CO2/CH4}$ = 44.8, $\alpha_{CO2/N2}$ = 35.1	[132]
PVAm	PEG-UiO-66-NH_2	0.3 MPa, 25 °C, mixed gas	CO_2/N_2	P_{CO2} = 1 295 GPU, $\alpha_{CO2/N2}$ = 91	[133]
Polynorbornene	UiO-66-NH_2-ND	0.3 MPa, 30 °C, single gas	H_2/CO_2	P_{H2} = 213.2 Barrer, $\alpha_{H2/CO2}$ = 6.8	[137]
PEG/PPG–PDMS	UiO-66-NB	0.1 MPa, 30 °C, single gas	CO_2/N_2	P_{CO2} = 585 Barrer, $\alpha_{CO2/N2}$ = 53	[29]

MA: methacrylic anhydride.

via an ultraviolet (UV)-induced radical polymerization (Fig. 14) [139]. With only 1 wt% of MOC added, the obtained hybrid membrane exhibited an improved CO_2 permeability without compromising CO_2/CH_4 selectivity. The addition of MOCs helped to increase CO_2 solubility and diffusivity, as confirmed by sorption analysis. Since the membranes could be cured quickly under UV treatment, MOC aggregation could be avoided during the membrane fabrication process. The fluorescence technique provided evidence for the structural integrity and homogeneous distribution of the MOCs within the membrane architecture at the molecular level. This crosslinking method is expected to be applicable to other types of MOCs with different topologies and pore sizes, yielding defect-free membranes with high loadings. Considering the analogous crystal engineering of MOFs and MOCs, strategies adopted in constructing MOF-based covalently bonded MMMs may also be extended to fabricate MOC-based covalently bonded MMMs. For example, MOCs with $-NH_2$ groups are expected to crosslink with isocyanate-terminated oligomers or epoxy group-terminated oligomers to fabricate crosslinked MMMs under mild conditions [133,140].

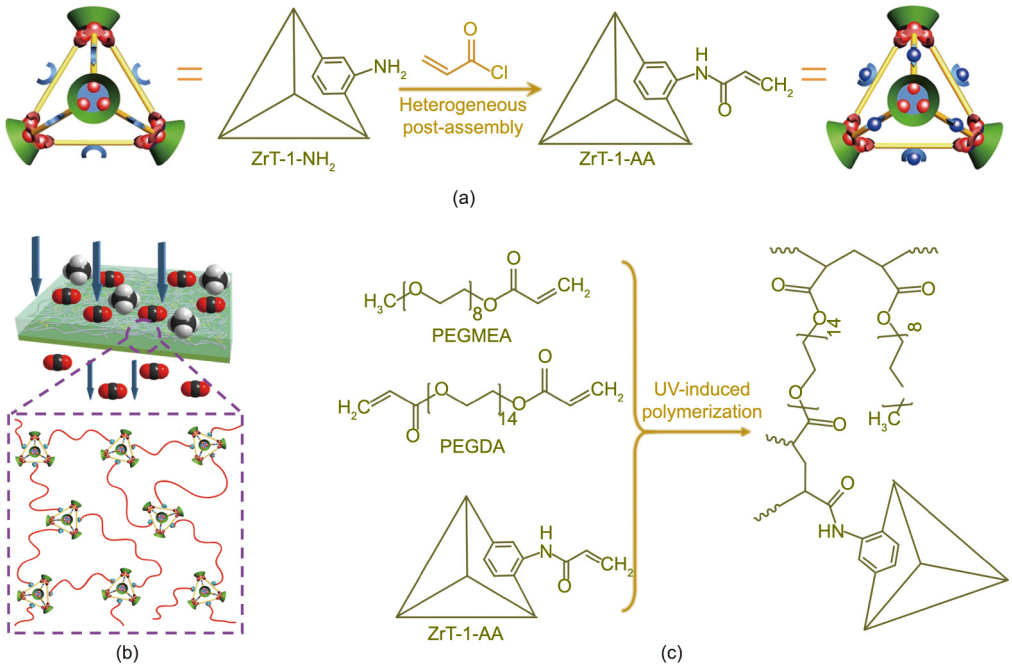

Fig. 14. (a) Synthetic route of ZrT-1-AA. (b) Schematic diagram and (c) synthetic route of HHMs constructed by polymerizable ZrT-1-AA and PEO polymers. PEGMEA: poly(ethylene glycol) methyl ether acrylate; PEGDA: poly(ethylene glycol) diacrylate; Reproduced from Ref. [139] with permission.

4. Challenges and perspectives

4.1. Extension of gas separation applications

Existing studies on MMMs mainly focus on CO_2-related separations, including CO_2/N_2, CO_2/CH_4, and H_2/CO_2 separations. Future work is encouraged to extend applications to more challenging separations such as C_2H_4/C_2H_6 and C_3H_6/C_3H_8 separations [43,141,142]. In addition to focusing on commonly studied porous materials such as ZIF-8 and ZIF-67 for C_3H_6/C_3H_8 separation, it is recommended to propose novel strategies and exploit more advanced porous materials and membrane materials. The construction of favorable sorption sites for C_2H_4 or C_3H_6 in MOFs (e.g., defective MOF, MOF/ionic liquid composite) would be conducive to improving C_2H_4/C_2H_6 or C_3H_6/C_3H_8 separation selectivity [105,124]. The fabrication of ultrahigh MOF-based MMMs will help to enhance gas permeability and fully utilize the characteristics of porous materials.

4.2. Fabrication of ultrathin MMMs

Although dense MMM materials with inspiring separation performance have been greatly exploited, the fabrication of ultrathin MMMs (less than 1 μm thick) with high permeance and selectivity is highly desirable for large-scale industrial applications [7,143]. When fabricating ultrathin MMMs, the interfacial compatibility and other issues in dense MMMs may be magnified. For example, it has been demonstrated that ultrathin membranes may undergo an accelerated aging process in comparison with dense membranes [144]. Since the membrane becomes thinner, porous fillers with smaller particle sizes (i.e., less than 20 nm) will be conducive to eliminating undesirable interface issues and maintaining separation selectivity. In this case, discrete MOCs will be more promising than bulky MOF particles, since the particle size of MOCs is usually less than 10 nm. The development of advanced membrane fabrication techniques is also crucial for preparing defect-free ultrathin MMMs. Interfacial polymerization (IP), gravity-induced interface self-assembly, or ATRP-based CAP techniques may help in the fabrication of ultrathin MMMs [11].

4.3. Exploitation of characterization methods

With the increased complexity of fabricated MMMs, there is a need to improve characterization techniques in order to better understand and regulate the dispersity of porous fillers within polymeric matrixes. In general, it is relatively easy to characterize a crystalline MOF lattice within an amorphous polymer using traditional techniques, such as transmission electron microscopy (TEM) and powder X-ray diffraction (PXRD). However, it is not straightforward to characterize MOCs, due to their monodispersity and nanoscale particle size. In this case, FIB-SEM or focused ion beam transmission electron microscopy (FIB-TEM) affords a comprehensive visualization of the filler orientation and dispersion at the nanoscale level [125,126,145,146]. Fluorescence techniques can provide a three-dimensional (3D) resolution of membrane structures in order to demonstrate the structural integrity of MOCs within a matrix, although only a subset of MOCs exhibit intrinsic fluorescence [139,147]. In addition, the accessible porosity of fillers within a polymeric matrix cannot be directly proven by these methods. Positron annihilation lifetime spectroscopy (PALS) is a widely accepted technique for determining the pore size distribution, although it may not be available to all researchers. Exploring other auxiliary techniques (e.g., Raman spectroscopy) is necessary in order to gain more information on the pore size distribution. Understanding the interfacial interactions between porous fillers and a polymeric matrix is also necessary in order to guide material design and fully exploit the potential of each component. Solid-state nuclear magnetic resonance (ssNMR) is a powerful technique for unveiling molecular-level interactions between porous fillers and polymers but may be limited by a high concentration of polymer [31,135,148,149]. The synergistic application of characterizations and molecular simulations is highly desirable in order to elucidate the interfacial interactions within MMMs at an atomistic level [150].

4.4. Study of the structure–performance relationship

Although extensive experiments have been carried out to evaluate the gas separation performance of MMMs, the structure–performance relationship between the intrinsic properties of MOFs or MOCs and the gas performance of their MMMs has not yet been fully understood, and it is time-consuming to investigate the tremendous expanse of combinations solely by experiments. To address this issue, a combination of computation (e.g., grand canonical Monte Carlo simulation) and experiments will be helpful in finding effective predictors of membrane performance [143,151,152]. In addition to computer simulation, the exploitation of machine learning, which is a class of statistical models that predicts properties based on a set of data, would provide a significant advantage to researchers in the assessment of the structure–performance relationship of membrane materials, since machine learning requires neither specialized equipment and experimental environments nor expensive computing clusters and supercomputers [153]. Machine learning has been utilized to discover novel polymers and predict the gas permeability of polymer membranes [153–155]. We believe that it is possible to extend machine learning to predict the separation performance of MMMs at an early stage of experimental activities and thereby help accelerate the design of membrane materials and membrane process engineering.

5. Conclusions

In conclusion, MMMs with MOFs and MOCs as porous materials have demonstrated prominent achievements in membrane-based gas separation. Although these two types of materials share many similarities, MOFs are more popular than MOCs in MMM fabrication to date, and the importance of MOCs in MMMs remains to be explored. Developing strong interactions between MOFs/MOCs and polymeric matrixes by forming electrostatic interactions, hydrogen bonds, coordination bonds, or covalent bonds is important to enhance the interfacial compatibility and improve the gas separation performance of the resulting MMMs. A deep understanding of the structure–performance relationship of MMMs, the exploitation of advanced characterization techniques and ultrathin MMMs, and the extension of applications to more challenging gas separations are also required in order to promote the widespread development of MMMs in the future.

Acknowledgments

This work was supported by the Ministry of Education, Singapore (MOE2019-T2-1-093 and MOE-T2EP10122-0002), the Energy Market Authority of Singapore (EMA-EP009-SEGC-020), the Agency for Science, Technology and Research (U2102d2004 and U2102d2012), and the National Research Foundation Singapore (NRF-CRP26-2021RS-0002).

Compliance with ethics guidelines

Ziqi Yang, Zhongjie Wu, Shing Bo Peh, Yunpan Ying, Hao Yang, and Dan Zhao declare that they have no conflict of interest or financial conflicts to disclose.

References

[1] Koros WJ, Zhang C. Materials for next-generation molecularly selective synthetic membranes. Nat Mater 2017;16(3):289–97.
[2] Zhang Y, Sunarso J, Liu S, Wang R. Current status and development of membranes for CO_2/CH_4 separation: a review. Int J Greenh Gas Control 2013;12:84–107.
[3] Bernardo P, Drioli E, Golemme G. Membrane gas separation: a review/state of the art. Ind Eng Chem Res 2009;48(10):4638–63.
[4] Brunetti A, Scura F, Barbieri G, Drioli E. Membrane technologies for CO_2 separation. J Membr Sci 2010;359(1–2):115–25.
[5] Baker RW, Low BT. Gas separation membrane materials: a perspective. Macromolecules 2014;47(20):6999–7013.
[6] Dechnik J, Sumby CJ, Janiak C. Enhancing mixed-matrix membrane performance with metal–organic framework additives. Cryst Growth Des 2017;17(8):4467–88.
[7] Wang S, Li X, Wu H, Tian Z, Xin Q, He G, et al. Advances in high permeability polymer-based membrane materials for CO_2 separations. Energy Environ Sci 2016;9(6):1863–90.
[8] Rufford TE, Smart S, Watson GCY, Graham BF, Boxall J, Diniz da Costa JC, et al. The removal of CO_2 and N_2 from natural gas: a review of conventional and emerging process technologies. J Petrol Sci Eng 2012;94–95:123–54.
[9] Lokhandwala KA, Pinnau I, He Z, Amo KD, DaCosta AR, Wijmans JG, et al. Membrane separation of nitrogen from natural gas: a case study from membrane synthesis to commercial deployment. J Membr Sci 2010;346(2):270–9.
[10] Hosseini SS, Chung TS. Carbon membranes from blends of PBI and polyimides for N_2/CH_4 and CO_2/CH_4 separation and hydrogen purification. J Membr Sci 2009;328(1–2):174–85.
[11] Xie K, Fu Q, Qiao GG, Webley PA. Recent progress on fabrication methods of polymeric thin film gas separation membranes for CO_2 capture. J Membr Sci 2019;572:38–60.
[12] Venna SR, Carreon MA. Metal organic framework membranes for carbon dioxide separation. Chem Eng Sci 2015;124:3–19.
[13] Lin R, Villacorta Hernandez B, Ge L, Zhu Z. Metal organic framework based mixed matrix membranes: an overview on filler/polymer interfaces. J Mater Chem A 2018;6(2):293–312.
[14] Liang CZ, Chung TS, Lai JY. A review of polymeric composite membranes for gas separation and energy production. Prog Polym Sci 2019;97:101141.
[15] Li W. Metal–organic framework membranes: production, modification, and applications. Prog Mater Sci 2019;100:21–63.
[16] Ying Y, Tong M, Ning S, Ravi SK, Peh SB, Tan SC, et al. Ultrathin two-dimensional membranes assembled by ionic covalent organic nanosheets with reduced apertures for gas separation. J Am Chem Soc 2020;142(9):4472–80.
[17] Ying Y, Peh SB, Yang H, Yang Z, Zhao D. Ultrathin covalent organic framework membranes via a multi-interfacial engineering strategy for gas separation. Adv Mater 2022;34(25):e2104946.
[18] Ying Y, Zhang Z, Peh SB, Karmakar A, Cheng Y, Zhang J, et al. Pressure-responsive two–dimensional metal–organic framework composite membranes for CO_2 separation. Angew Chem Int Ed Engl 2021;60(20):11318–25.
[19] Wang X, Chi C, Zhang K, Qian Y, Gupta KM, Kang Z, et al. Reversed thermo-switchable molecular sieving membranes composed of two-dimensional metal–organic nanosheets for gas separation. Nat Commun 2017;8(1):14460.
[20] Sandru M, Sandru EM, Ingram WF, Deng J, Stenstad PM, Deng L, et al. An integrated materials approach to ultrapermeable and ultraselective CO_2 polymer membranes. Science 2022;376(6588):90–4.
[21] Robeson LM. Correlation of separation factor versus permeability for polymeric membranes. J Membr Sci 1991;62(2):165–85.
[22] Robeson LM. The upper bound revisited. J Membr Sci 2008;320(1–2):390–400.
[23] Comesaña-Gándara B, Chen J, Bezzu CG, Carta M, Rose I, Ferrari MC, et al. Redefining the Robeson upper bounds for CO_2/CH_4 and CO_2/N_2 separations using a series of ultrapermeable benzotriptycene-based polymers of intrinsic microporosity. Energy Environ Sci 2019;12(9):2733–40.
[24] Pastore VJ, Cook TR. Coordination-driven self-assembly in polymer–inorganic hybrid materials. Chem Mater 2020;32(9):3680–700.
[25] Dechnik J, Gascon J, Doonan CJ, Janiak C, Sumby CJ. Mixed-matrix membranes. Angew Chem Int Ed Engl 2017;56(32):9292–310.
[26] Cheng Y, Ying Y, Japip S, Jiang SD, Chung TS, Zhang S, et al. Advanced porous materials in mixed matrix membranes. Adv Mater 2018;30(47):1802401.
[27] Guo X, Qiao Z, Liu D, Zhong C. Mixed-matrix membranes for CO_2 separation: role of the third component. J Mater Chem A 2019;7(43):24738–59.
[28] Muthukumaraswamy Rangaraj V, Wahab MA, Reddy KSK, Kakosimos G, Abdalla O, Favvas EP, et al. Metal organic framework-based mixed matrix membranes for carbon dioxide separation: recent advances and future directions. Front Chem 2020;8:534.
[29] Hossain I, Husna A, Chaemchuen S, Verpoort F, Kim TH. Cross-linked mixed-matrix membranes using functionalized UiO-66-NH_2 into PEG/PPG–PDMS-based rubbery polymer for efficient CO_2 separation. ACS Appl Mater Interfaces 2020;12(52):57916–31.
[30] Li C, Wu C, Zhang B. Enhanced CO_2/CH_4 separation performances of mixed matrix membranes incorporated with two-dimensional Ni-based MOF nanosheets. ACS Sustain Chem Eng 2020;8(1):642–8.
[31] Semino R, Moreton JC, Ramsahye NA, Cohen SM, Maurin G. Understanding the origins of metal–organic framework/polymer compatibility. Chem Sci 2018;9(2):315–24.
[32] Nordin NAHM, Ismail AF, Mustafa A, Murali RS, Matsuura T. The impact of ZIF-8 particle size and heat treatment on CO_2/CH_4 separation using asymmetric mixed matrix membrane. RSC Adv 2014;4(94):52530–41.
[33] Cheng Y, Wang Z, Zhao D. Mixed matrix membranes for natural gas upgrading: current status and opportunities. Ind Eng Chem Res 2018;57(12):4139–69.

[34] Wang B, Sheng M, Xu J, Zhao S, Wang J, Wang Z. Recent advances of gas transport channels constructed with different dimensional nanomaterials in mixed-matrix membranes for CO_2 separation. Small Methods 2020;4(3):1900749.
[35] Zhu X, Tian C, Do-Thanh CL, Dai S. Two-dimensional materials as prospective scaffolds for mixed-matrix membrane-based CO_2 separation. ChemSusChem 2017;10(17):3304–16.
[36] Zhu G, O'Nolan D, Lively RP. Molecularly mixed composite membranes: challenges and opportunities. Chemistry Eur J 2020;26(16):3464–73.
[37] Bushell AF, Budd PM, Attfield MP, Jones JTA, Hasell T, Cooper AI, et al. Nanoporous organic polymer/cage composite membranes. Angew Chem Int Ed Engl 2013;52(4):1253–6.
[38] Bai Y, Dou Y, Xie LH, Rutledge W, Li JR, Zhou HC. Zr-based metal–organic frameworks: design, synthesis, structure, and applications. Chem Soc Rev 2016;45(8):2327–67.
[39] Zhou HC, Long JR, Yaghi OM. Introduction to metal–organic frameworks. Chem Rev 2012;112(2):673–4.
[40] Furukawa H, Cordova KE, O'Keeffe M, Yaghi OM. The chemistry and applications of metal–organic frameworks. Science 2013;341(6149):1230444.
[41] Askari M, Chung TS. Natural gas purification and olefin/paraffin separation using thermal cross-linkable co-polyimide/ZIF-8 mixed matrix membranes. J Membr Sci 2013;444:173–83.
[42] Lee YR, Jang MS, Cho HY, Kwon HJ, Kim S, Ahn WS. ZIF-8: a comparison of synthesis methods. Chem Eng J 2015;271:276–80.
[43] Zhang C, Dai Y, Johnson JR, Karvan O, Koros WJ. High performance ZIF-8/6FDA–DAM mixed matrix membrane for propylene/propane separations. J Membr Sci 2012;389:34–42.
[44] Yang T, Chung TS. Room-temperature synthesis of ZIF-90 nanocrystals and the derived nano-composite membranes for hydrogen separation. J Mater Chem A 2013;1(19):6081–90.
[45] Xiang L, Sheng L, Wang C, Zhang L, Pan Y, Li Y. Amino-functionalized ZIF-7 nanocrystals: improved intrinsic separation ability and interfacial compatibility in mixed-matrix membranes for CO_2 /CH_4 separation. Adv Mater 2017;29(32):1606999.
[46] Fan Y, Yu H, Xu S, Shen Q, Ye H, Li N. Zn(II)-modified imidazole containing polyimide/ZIF-8 mixed matrix membranes for gas separations. J Membr Sci 2020;597:117775.
[47] Yu J, Wang C, Xiang L, Xu Y, Pan Y. Enhanced C_3H_6/C_3H_8 separation performance in poly(vinyl acetate) membrane blended with ZIF-8 nanocrystals. Chem Eng Sci 2018;179:1–12.
[48] Ma X, Swaidan RJ, Wang Y, Hsiung C, Han Y, Pinnau I. Highly compatible hydroxyl-functionalized microporous polyimide-ZIF-8 mixed matrix membranes for energy efficient propylene/propane separation. ACS Appl Nano Mater 2018;1(7):3541–7.
[49] Hu Z, Faucher S, Zhuo Y, Sun Y, Wang S, Zhao D. Combination of optimization and metalated-ligand exchange: an effective approach to functionalize UiO-66(Zr) MOFs for CO_2 separation. Chem Eur J 2015;21(48):17246–55.
[50] Hu Z, Peng Y, Gao Y, Qian Y, Ying S, Yuan D, et al. Direct synthesis of hierarchically porous metal–organic frameworks with high stability and strong brønsted acidity: the decisive role of hafnium in efficient and selective fructose dehydration. Chem Mater 2016;28(8):2659–67.
[51] Hu Z, Wang Y, Farooq S, Zhao D. A highly stable metal–organic framework with optimum aperture size for CO_2 capture. AlChE J 2017;63(9):4103–14.
[52] Prasetya N, Donose BC, Ladewig BP. A new and highly robust light-responsive Azo-UiO-66 for highly selective and low energy post-combustion CO_2 capture and its application in a mixed matrix membrane for CO_2/N_2 separation. J Mater Chem A 2018;6(34):16390–402.
[53] Peh SB, Wang Y, Zhao D. Scalable and sustainable synthesis of advanced porous materials. ACS Sustain Chem Eng 2019;7(4):3647–70.
[54] Feng L, Hou HB, Zhou H. UiO-66 derivatives and their composite membranes for effective proton conduction. Dalton Trans 2020;49(47):17130–9.
[55] Peh SB, Karmakar A, Zhao D. Multiscale design of flexible metal–organic frameworks. Trends Chem 2020;2(3):199–213.
[56] Sabetghadam A, Seoane B, Keskin D, Duim N, Rodenas T, Shahid S, et al. Metal organic framework crystals in mixed-matrix membranes: impact of the filler morphology on the gas separation performance. Adv Funct Mater 2016;26(18):3154–63.
[57] Xin Q, Ouyang J, Liu T, Li Z, Li Z, Liu Y, et al. Enhanced interfacial interaction and CO_2 separation performance of mixed matrix membrane by incorporating polyethylenimine-decorated metal–organic frameworks. ACS Appl Mater Interfaces 2015;7(2):1065–77.
[58] Schneemann A, Bon V, Schwedler I, Senkovska I, Kaskel S, Fischer RA. Flexible metal–organic frameworks. Chem Soc Rev 2014;43(16):6062–96.
[59] Férey G, Mellot-Draznieks C, Serre C, Millange F, Dutour J, Surblé S, et al. A chromium terephthalate-based solid with unusually large pore volumes and surface area. Science 2005;309(5743):2040–2.
[60] Hosono N, Kitagawa S. Modular design of porous soft materials via self-organization of metal–organic cages. Acc Chem Res 2018;51(10):2437–46.
[61] Lee S, Jeong H, Nam D, Lah MS, Choe W. The rise of metal–organic polyhedra. Chem Soc Rev 2021;50(1):528–55.
[62] Gosselin AJ, Rowland CA, Bloch ED. Permanently microporous metal–organic polyhedra. Chem Rev 2020;120(16):8987–9014.
[63] El-Sayed ESM, Yuan D. Metal–organic cages (MOCs): from discrete to cage-based extended architectures. Chem Lett 2020;49(1):28–53.
[64] Mollick S, Fajal S, Mukherjee S, Ghosh SK. Stabilizing metal–organic polyhedra (MOP): issues and strategies. Chem Asian J 2019;14(18):3096–108.
[65] Perez EV, Balkus Jr KJ, Ferraris JP, Musselman IH. Metal–organic polyhedra 18 mixed-matrix membranes for gas separation. J Membr Sci 2014;463:82–93.
[66] Liu G, Yuan YD, Wang J, Cheng Y, Peh SB, Wang Y, et al. Process-tracing study on the postassembly modification of highly stable zirconium metal–organic cages. J Am Chem Soc 2018;140(20):6231–4.
[67] Liu G, Ju Z, Yuan D, Hong M. *In situ* construction of a coordination zirconocene tetrahedron. Inorg Chem 2013;52(24):13815–7.
[68] Nam D, Huh J, Lee J, Kwak JH, Jeong HY, Choi K, et al. Cross-linking Zr-based metal–organic polyhedra via postsynthetic polymerization. Chem Sci 2017;8(11):7765–71.
[69] Xing WH, Li HY, Dong XY, Zang SQ. Robust multifunctional Zr-based metal–organic polyhedra for high proton conductivity and selective CO_2 capture. J Mater Chem A 2018;6(17):7724–30.
[70] Lee S, Lee JH, Kim JC, Lee S, Kwak SK, Choe W. Porous Zr_6L_3 metallocage with synergetic binding centers for CO_2. ACS Appl Mater Interfaces 2018;10(10):8685–91.
[71] Liu J, Duan W, Song J, Guo X, Wang Z, Shi X, et al. Self-healing hyper-cross-linked metal–organic polyhedra (HCMOPs) membranes with antimicrobial activity and highly selective separation properties. J Am Chem Soc 2019;141(30):12064–70.
[72] Liu G, Yang Z, Zhou M, Wang Y, Yuan D, Zhao D. Heterogeneous postassembly modification of zirconium metal–organic cages in supramolecular frameworks. Chem Commun 2021;57(51):6276–9.
[73] Li JR, Zhou HC. Bridging-ligand-substitution strategy for the preparation of metal–organic polyhedra. Nat Chem 2010;2(10):893–8.
[74] Eddaoudi M, Kim J, Wachter JB, Chae HK, O'Keeffe M, Yaghi OM. Porous metal–organic polyhedra: 25 Å cuboctahedron constructed from 12 $Cu_2(CO_2)_4$ paddle-wheel building blocks. J Am Chem Soc 2001;123(18):4368–9.
[75] Barreda O, Bannwart G, Yap GPA, Bloch ED. Ligand-based phase control in porous molecular assemblies. ACS Appl Mater Interfaces 2018;10(14):11420–4.
[76] Taggart GA, Antonio AM, Lorzing GR, Yap GPA, Bloch ED. Tuning the porosity, solubility, and gas-storage properties of cuboctahedral coordination cages via amide or ester functionalization. ACS Appl Mater Interfaces 2020;12(22):24913–9.
[77] Tonigold M, Volkmer D. Comparative solvolytic stabilities of copper(II) nanoballs and dinuclear Cu(II) paddle wheel units. Inorg Chim Acta 2010;363(15):4220–9.
[78] Yun YN, Sohail M, Moon JH, Kim TW, Park KM, Chun DH, et al. Defect-free mixed-matrix membranes with hydrophilic metal–organic polyhedra for efficient carbon dioxide separation. Chem Asian J 2018;13(6):631–5.
[79] Hosono N, Guo W, Omoto K, Yamada H, Kitagawa S. Bottom-up synthesis of defect-free mixed-matrix membranes by using polymer-grafted metal–organic polyhedra. Chem Lett 2019;48(6):597–600.
[80] Vetromile CM, Lozano A, Feola S, Larsen RW. Solution stability of Cu(II) metal–organic polyhedra. Inorg Chim Acta 2011;378(1):36–41.
[81] Zhao J, Yan X. Rh(II)-based metal–organic polyhedra. Chem Lett 2020;49(6):659–65.
[82] Carné-Sánchez A, Albalad J, Grancha T, Imaz I, Juanhuix J, Larpent P, et al. Postsynthetic covalent and coordination functionalization of rhodium(II)-based metal–organic polyhedra. J Am Chem Soc 2019;141(9):4094–102.
[83] Carné-Sánchez A, Craig GA, Larpent P, Guillerm V, Urayama K, Maspoch D, et al. A coordinative solubilizer method to fabricate soft porous materials from insoluble metal–organic polyhedra. Angew Chem Int Ed Engl 2019;58(19):6347–50.
[84] Percástegui EG, Ronson TK, Nitschke JR. Design and applications of water-soluble coordination cages. Chem Rev 2020;120(24):13480–544.
[85] Zhao D, Tan S, Yuan D, Lu W, Rezenom YH, Jiang H, et al. Surface functionalization of porous coordination nanocages via click chemistry and their application in drug delivery. Adv Mater 2011;23(1):90–3.
[86] Niu Z, Wang L, Fang S, Lan PC, Aguila B, Perman J, et al. Solvent-assisted coordination driven assembly of a supramolecular architecture featuring two types of connectivity from discrete nanocages. Chem Sci 2019;10(27):6661–5.
[87] Shah Buddin MMH, Ahmad AL. A review on metal–organic frameworks as filler in mixed matrix membrane: recent strategies to surpass upper bound for CO_2 separation. J CO_2 Util 2021;51:101616.
[88] He S, Zhu B, Li S, Zhang Y, Jiang X, Lau CH, et al. Recent progress in PIM-1 based membranes for sustainable CO_2 separations: polymer structure manipulation and mixed matrix membrane design. Separ Purif Tech 2022;284:120277.
[89] Wu X, Liu W, Wu H, Zong X, Yang L, Wu Y, et al. Nanoporous ZIF-67 embedded polymers of intrinsic microporosity membranes with enhanced gas separation performance. J Membr Sci 2018;548:309–18.
[90] Japip S, Xiao Y, Chung TS. Particle-size effects on gas transport properties of 6FDA–durene/ZIF-71 mixed matrix membranes. Ind Eng Chem Res 2016;55(35):9507–17.
[91] Ghalei B, Sakurai K, Kinoshita Y, Wakimoto K, Isfahani AP, Song Q, et al. Enhanced selectivity in mixed matrix membranes for CO_2 capture through efficient dispersion of amine-functionalized MOF nanoparticles. Nat Energy 2017;2(7):17086.
[92] Ye C, Wu X, Wu H, Yang L, Ren Y, Wu Y, et al. Incorporating nano-sized ZIF-67 to enhance selectivity of polymers of intrinsic microporosity membranes for biogas upgrading. Chem Eng Sci 2020;216:115497.

[93] He S, Zhu B, Jiang X, Han G, Li S, Lau CH, et al. Symbiosis-inspired *de novo* synthesis of ultrahigh MOF growth mixed matrix membranes for sustainable carbon capture. Proc Natl Acad Sci USA 2022;119(1):e2114964119.
[94] Yang F, Mu H, Wang C, Xiang L, Yao KX, Liu L, et al. Morphological map of ZIF-8 crystals with five distinctive shapes: feature of filler in mixed-matrix membranes on C_3H_6/C_3H_8 separation. Chem Mater 2018;30(10):3467–73.
[95] Wu X, Ren Y, Sui G, Wang G, Xu G, Yang L, et al. Accelerating CO_2 capture of highly permeable polymer through incorporating highly selective hollow zeolite imidazolate framework. AlChE J 2020;66(2):e16800.
[96] Shen J, Liu G, Huang K, Li Q, Guan K, Li Y, et al. UiO-66-polyether block amide mixed matrix membranes for CO_2 separation. J Membr Sci 2016;513:155–65.
[97] Ma C, Urban JJ. Hydrogen-bonded polyimide/metal–organic framework hybrid membranes for ultrafast separations of multiple gas pairs. Adv Funct Mater 2019;29(32):1903243.
[98] Chen XY, Vinh-Thang H, Rodrigue D, Kaliaguine S. Amine-functionalized MIL-53 metal–organic framework in polyimide mixed matrix membranes for CO_2/CH_4 separation. Ind Eng Chem Res 2012;51(19):6895–906.
[99] Zhu H, Wang L, Jie X, Liu D, Cao Y. Improved interfacial affinity and CO_2 separation performance of asymmetric mixed matrix membranes by incorporating postmodified MIL-53(Al). ACS Appl Mater Interfaces 2016;8(34):22696–704.
[100] Seoane B, Téllez C, Coronas J, Staudt C. NH_2-MIL-53(Al) and NH_2-MIL-101(Al) in sulfur-containing copolyimide mixed matrix membranes for gas separation. Separ Purif Tech 2013;111:72–81.
[101] Yu G, Zou X, Sun L, Liu B, Wang Z, Zhang P, et al. Constructing connected paths between UiO-66 and PIM-1 to improve membrane CO_2 separation with crystal-like gas selectivity. Adv Mater 2019;31(15):1806853.
[102] Venna SR, Lartey M, Li T, Spore A, Kumar S, Nulwala HB, et al. Fabrication of MMMs with improved gas separation properties using externally-functionalized MOF particles. J Mater Chem A 2015;3(9):5014–22.
[103] Thür R, Van Velthoven N, Lemmens V, Bastin M, Smolders S, De Vos D, et al. Modulator-mediated functionalization of MOF-808 as a platform tool to create high-performance mixed-matrix membranes. ACS Appl Mater Interfaces 2019;11(47):44792–801.
[104] Jiang Y, Liu C, Caro J, Huang A. A new UiO-66-NH_2 based mixed-matrix membranes with high CO_2/CH_4 separation performance. Microporous Mesoporous Mater 2019;274:203–11.
[105] Hillman F, Hamid MRA, Krokidas P, Moncho S, Brothers EN, Economou IG, et al. Delayed linker addition (DLA) synthesis for hybrid SOD ZIFs with unsubstituted imidazolate linkers for propylene/propane and *n*-butane/*i*-butane separations. Angew Chem Int Ed Engl 2021;60(18):10103–11.
[106] Wu MX, Wang Y, Zhou G, Liu X. Core–shell MOFs@MOFs: diverse designability and enhanced selectivity. ACS Appl Mater Interfaces 2020;12(49):54285–305.
[107] Song Z, Qiu F, Zaia EW, Wang Z, Kunz M, Guo J, et al. Dual-channel, molecular-sieving core/shell ZIF@MOF architectures as engineered fillers in hybrid membranes for highly selective CO_2 separation. Nano Lett 2017;17(11):6752–8.
[108] Cheng Y, Ying Y, Zhai L, Liu G, Dong J, Wang Y, et al. Mixed matrix membranes containing MOF@COF hybrid fillers for efficient CO_2/CH_4 separation. J Membr Sci 2019;573:97–106.
[109] Sánchez-Laínez J, Veiga A, Zornoza B, Balestra SRG, Hamad S, Ruiz-Salvador AR, et al. Tuning the separation properties of zeolitic imidazolate framework core–shell structures via post-synthetic modification. J Mater Chem A 2017;5(48):25601–8.
[110] Sánchez-Laínez J, Zornoza B, Orsi AF, Łozińska MM, Dawson DM, Ashbrook SE, et al. Synthesis of ZIF-93/11 hybrid nanoparticles via post-synthetic modification of ZIF-93 and their use for H_2/CO_2 separation. Chem Eur J 2018;24(43):11211–9.
[111] Yuan SH, Isfahani AP, Yamamoto T, Muchtar A, Wu CY, Huang G, et al. Nanosized core–shell zeolitic imidazolate frameworks-based membranes for gas separation. Small Methods 2020;4(8):2000021.
[112] Wu C, Zhang K, Wang H, Fan Y, Zhang S, He S, et al. Enhancing the gas separation selectivity of mixed-matrix membranes using a dual-interfacial engineering approach. J Am Chem Soc 2020;142(43):18503–12.
[113] Li C, Liu J, Zhang K, Zhang S, Lee Y, Li T. Coating the right polymer: achieving ideal metal–organic framework particle dispersibility in polymer matrixes using a coordinative crosslinking surface modification method. Angew Chem Int Ed Engl 2021;60(25):14138–45.
[114] Wang Z, Wang D, Zhang S, Hu L, Jin J. Interfacial design of mixed matrix membranes for improved gas separation performance. Adv Mater 2016;28(17):3399–405.
[115] Wang B, Qiao Z, Xu J, Wang J, Liu X, Zhao S, et al. Unobstructed ultrathin gas transport channels in composite membranes by interfacial self-assembly. Adv Mater 2020;32(22):1907701.
[116] Wang H, He S, Qin X, Li C, Li T. Interfacial engineering in metal–organic framework-based mixed matrix membranes using covalently grafted polyimide brushes. J Am Chem Soc 2018;140(49):17203–10.
[117] Qian Q, Wu AX, Chi WS, Asinger PA, Lin S, Hypsher A, et al. Mixed-matrix membranes formed from imide-functionalized UiO-66-NH_2 for improved interfacial compatibility. ACS Appl Mater Interfaces 2019;11(34):31257–69.
[118] Dai D, Wang H, Li C, Qin X, Li T. A physical entangling strategy for simultaneous interior and exterior modification of metal–organic framework with polymers. Angew Chem Int Ed Engl 2021;60(13):7389–96.
[119] Guo X, Huang H, Liu D, Zhong C. Improving particle dispersity and CO_2 separation performance of amine-functionalized CAU-1 based mixed matrix membranes with polyethyleneimine-grafting modification. Chem Eng Sci 2018;189:277–85.
[120] Wang B, Xu J, Wang J, Zhao S, Liu X, Wang Z. High-performance membrane with angstrom-scale manipulation of gas transport channels via polymeric decorated MOF cavities. J Membr Sci 2021;625:119175.
[121] Wang H, Ni Y, Dong Z, Zhao Q. A mechanically enhanced metal–organic framework/PDMS membrane for CO_2/N_2 separation. React Funct Polym 2021;160:104825.
[122] Xie K, Fu Q, Kim J, Lu H, He Y, Zhao Q, et al. Increasing both selectivity and permeability of mixed-matrix membranes: sealing the external surface of porous MOF nanoparticles. J Membr Sci 2017;535:350–6.
[123] Yang Z, Ying Y, Pu Y, Wang D, Yang H, Zhao D. Poly(ionic liquid)-functionalized UiO-66-$(OH)_2$: improved interfacial compatibility and separation ability in mixed matrix membranes for CO_2 separation. Ind Eng Chem Res 2022;61(22):7626–33.
[124] Lee TH, Jung JG, Kim YJ, Roh JS, Yoon HW, Ghanem BS, et al. Defect engineering in metal–organic frameworks towards advanced mixed matrix membranes for efficient propylene/propane separation. Angew Chem Int Ed Engl 2021;60(23):13081–8.
[125] Liu X, Wang X, Bavykina AV, Chu L, Shan M, Sabetghadam A, et al. Molecular-scale hybrid membranes derived from metal–organic polyhedra for gas separation. ACS Appl Mater Interfaces 2018;10(25):21381–9.
[126] Kitchin M, Teo J, Konstas K, Lau CH, Sumby CJ, Thornton AW, et al. AIMs: a new strategy to control physical aging and gas transport in mixed-matrix membranes. J Mater Chem A 2015;3(29):15241–7.
[127] Liu J, Fulong CRP, Hu L, Huang L, Zhang G, Cook TR, et al. Interpenetrating networks of mixed matrix materials comprising metal–organic polyhedra for membrane CO_2 capture. J Membr Sci 2020;606:118122.
[128] Sohail M, An H, Choi W, Singh J, Yim K, Kim BH, et al. Sorption-enhanced thin film composites with metal–organic polyhedral nanocages for CO_2 separation. J Membr Sci 2021;620:118826.
[129] Fulong CRP, Liu J, Pastore VJ, Lin H, Cook TR. Mixed-matrix materials using metal–organic polyhedra with enhanced compatibility for membrane gas separation. Dalton Trans 2018;47(24):7905–15.
[130] Ma J, Ying Y, Yang Q, Ban Y, Huang H, Guo X, et al. Mixed-matrix membranes containing functionalized porous metal–organic polyhedrons for the effective separation of CO_2–CH_4 mixture. Chem Commun 2015;51(20):4249–51.
[131] Tien-Binh N, Vinh-Thang H, Chen XY, Rodrigue D, Kaliaguine S. Crosslinked MOF–polymer to enhance gas separation of mixed matrix membranes. J Membr Sci 2016;520:941–50.
[132] Lin R, Ge L, Hou L, Strounina E, Rudolph V, Zhu Z. Mixed matrix membranes with strengthened MOFs/polymer interfacial interaction and improved membrane performance. ACS Appl Mater Interfaces 2014;6(8):5609–18.
[133] Xu R, Wang Z, Wang M, Qiao Z, Wang J. High nanoparticles loadings mixed matrix membranes via chemical bridging-crosslinking for CO_2 separation. J Membr Sci 2019;573:455–64.
[134] Chen Z, Yan D, Ma L, Zhang Y, Zhang J, Li H, et al. Polymerizable metal–organic frameworks for the preparation of mixed matrix membranes with enhanced interfacial compatibility. iScience 2021;24(6):102560.
[135] Jiang X, Li S, He S, Bai Y, Shao L. Interface manipulation of CO_2-philic composite membranes containing designed UiO-66 derivatives towards highly efficient CO_2 capture. J Mater Chem A 2018;6(31):15064–73.
[136] Katayama Y, Bentz KC, Cohen SM. Defect-free MOF-based mixed-matrix membranes obtained by corona cross-linking. ACS Appl Mater Interfaces 2019;11(13):13029–37.
[137] Gao X, Zhang J, Huang K, Zhang J. ROMP for metal–organic frameworks: an efficient technique toward robust and high-separation performance membranes. ACS Appl Mater Interfaces 2018;10(40):34640–5.
[138] Harris K, Fujita D, Fujita M. Giant hollow M_nL_{2n} spherical complexes: structure, functionalisation and applications. Chem Commun 2013;49(60):6703–12.
[139] Yang Z, Liu G, Yuan YD, Peh SB, Ying Y, Fan W, et al. Homoporous hybrid membranes containing metal–organic cages for gas separation. J Membr Sci 2021;636:119564.
[140] Yao BJ, Jiang WL, Dong Y, Liu ZX, Dong YB. Post-synthetic polymerization of UiO-66-NH_2 nanoparticles and polyurethane oligomer toward stand-alone membranes for dye removal and separation. Chem Eur J 2016;22(30):10565–71.
[141] Liu D, Xiang L, Chang H, Chen K, Wang C, Pan Y, et al. Rational matching between MOFs and polymers in mixed matrix membranes for propylene/propane separation. Chem Eng Sci 2019;204:151–60.
[142] Dou H, Xu M, Wang B, Zhang Z, Luo D, Shi B, et al. Analogous mixed matrix membranes with self-assembled interface pathways. Angew Chem Int Ed Engl 2021;60(11):5864–70.
[143] Hu L, Clark K, Alebrahim T, Lin H. Mixed matrix membranes for post-combustion carbon capture: from materials design to membrane engineering. J Membr Sci 2022;644:120140.
[144] Tiwari RR, Jin J, Freeman BD, Paul DR. Physical aging, CO_2 sorption and plasticization in thin films of polymer with intrinsic microporosity (PIM-1). J Membr Sci 2017;537:362–71.
[145] Rodenas T, van Dalen M, García-Pérez E, Serra-Crespo P, Zornoza B, Kapteijn F, et al. Visualizing MOF mixed matrix membranes at the nanoscale: towards structure–performance relationships in CO_2/CH_4 separation over NH_2-MIL-53(Al)@PI. Adv Funct Mater 2014;24(2):249–56.

[146] Rodenas T, Luz I, Prieto G, Seoane B, Miro H, Corma A, et al. Metal–organic framework nanosheets in polymer composite materials for gas separation. Nat Mater 2015;14(1):48–55.
[147] Liu G, Zhang X, Yuan YD, Yuan H, Li N, Ying Y, et al. Thin-film nanocomposite membranes containing water-stable zirconium metal–organic cages for desalination. ACS Mater Lett 2021;3(3):268–74.
[148] Mileo PGM, Yuan S, Ayala Jr S, Duan P, Semino R, Cohen SM, et al. Structure of the polymer backbones in polyMOF materials. J Am Chem Soc 2020;142(24):10863–8.
[149] Duan P, Moreton JC, Tavares SR, Semino R, Maurin G, Cohen SM, et al. Polymer infiltration into metal–organic frameworks in mixed-matrix membranes detected *in situ* by NMR. J Am Chem Soc 2019;141(18):7589–95.
[150] Carja ID, Tavares SR, Shekhah O, Ozcan A, Semino R, Kale VS, et al. Insights into the enhancement of MOF/polymer adhesion in mixed-matrix membranes via polymer functionalization. ACS Appl Mater Interfaces 2021;13(24):29041–7.
[151] Semino R, Ramsahye NA, Ghoufi A, Maurin G. Microscopic model of the metal–organic framework/polymer interface: a first step toward understanding the compatibility in mixed matrix membranes. ACS Appl Mater Interfaces 2016;8(1):809–19.
[152] Thür R, Van Havere D, Van Velthoven N, Smolders S, Lamaire A, Wieme J, et al. Correlating MOF-808 parameters with mixed-matrix membrane (MMM) CO_2 permeation for a more rational MMM development. J Mater Chem A 2021;9(21):12782–96.
[153] Yuan Q, Longo M, Thornton AW, McKeown NB, Comesaña-Gándara B, Jansen JC, et al. Imputation of missing gas permeability data for polymer membranes using machine learning. J Membr Sci 2021;627:119207.
[154] Barnett JW, Bilchak CR, Wang Y, Benicewicz BC, Murdock LA, Bereau T, et al. Designing exceptional gas-separation polymer membranes using machine learning. Sci Adv 2020;6(20):eaaz4301.
[155] Wu S, Kondo Y, Kakimoto M, Yang B, Yamada H, Kuwajima I, et al. Machine-learning-assisted discovery of polymers with high thermal conductivity using a molecular design algorithm. npj Comput Mater 2019;5(1):66.